



Syntheses and evaluation of acridone-naphthalimide derivatives for regulating oncogene PDGFR- β expression

Meiling Zhang¹, Zuzhuang Wei¹, Xue Gong, Xiaoya Li, Shuangshuang Kang, Jing Wang, Bobo Liu, Zhi-Shu Huang, Ding Li^{*}

School of Pharmaceutical Sciences, Sun Yat-sen University, 132 Waihuang East Road, Guangzhou 510006, PR China

ARTICLE INFO

Keywords:

PDGFR- β
I-motif
G-quadruplex
Acridone
Naphthalimide
Cancer

ABSTRACT

Upregulation of platelet-derived growth factor receptor β (PDGFR- β) has been found to be associated with development of various types of cancers, which has become an attractive target for anti-tumor treatment. Previously, we have synthesized and studied an acridone derivative **B19**, which can selectively bind to and stabilize oncogene *c-myc* promoter i-motif, resulting in down-regulation of *c-myc* transcription and translation, however its effect on tumor cells apoptosis requires improvement. In the present study, we synthesized a variety of **B19** derivatives containing a known anti-cancer fluorescent chromophore naphthalimide for the purpose of enhancing anti-cancer activity. After screening, we found that acridone-naphthalimide derivative **WZZ02** could selectively stabilize PDGFR- β promoter G-quadruplex and destabilize its corresponding i-motif structure, without significant interaction to other oncogenes promoter G-quadruplex and i-motif. **WZZ02** down-regulated PDGFR- β gene transcription and translation in a dose-dependent manner, possibly due to above interactions. **WZZ02** could significantly inhibit cancer cell proliferation, and induce cell apoptosis and cycle arrest. **WZZ02** exhibited tumor growth inhibition activity in MCF-7 xenograft tumor model, which could be due to its binding interactions with PDGFR- β promoter G-quadruplex and i-motif. Our results suggested that **WZZ02** as a dual G-quadruplex/i-motif binder could be effective on both oncogene replication and transcription, which could become a promising lead compound for further development with improved potency and selectivity. The wide properties for the derivatives of 1,8-naphthalimide could facilitate further in-depth mechanistic studies of **WZZ02** through various fluorescent physical and chemical methods, which could help to further understand the function of PDGFR- β gene promoter G-quadruplex and i-motif.

1. Introduction

The platelet-derived growth factor receptor β (PDGFR- β) signaling pathway is a key regulator of cell proliferation and migration, and its overexpression can result in various diseases including cancer, vascular and fibrotic disorders.^{1–5} Current strategies for targeting PDGFR- β signaling pathway usually include inhibition of protein PDGFR- β receptor.⁶ Modulation of PDGFR- β at the transcriptional level provides an alternative approach of targeting the PDGFR- β signaling pathway for treatment of relevant diseases.⁷ It has been shown that a highly GC-rich region (–165 to –139) in human PDGFR- β promoter is an important regulatory element for PDGFR- β transcription.⁸ Traditional researches for regulating oncogene transcriptions usually focus on promoter DNA G-quadruplexes in oncogenes, such as *c-myc*,^{9,10} *vegf*,¹¹ *HIF-1 α* ,¹² *bcl-*

2,^{13,14} *k-ras*,¹⁵ *Rb*,¹⁶ *c-kit*,^{17,18} *RET*,¹⁹ *hTERT*,²⁰ which have been verified as transcriptional regulators^{21–23} formed in the proximal location of promoters under transcriptionally induced supercoiling. Their complementary C-rich sequences could form i-motif structures with intercalated hemiprotonated cytosine+–cytosine (C+–C) base pairs,^{24,25} however, biological roles of these i-motif structures have not been well studies so far. The formation of i-motifs varies over the cell cycle, with the highest level of formation occurring during late G1 phase, which is characterized by high levels of transcription and cellular growth. This is significantly different from G-quadruplex formation, which occurs predominantly during the DNA replication S phase, suggesting that the occurrence of i-motifs and G-quadruplexes are generally independent, and the i-motifs regulation in cell cycle might be more important than the G-quadruplexes regulation.²⁶

* Corresponding author.

E-mail address: liding@mail.sysu.edu.cn (D. Li).

¹ The first two authors made equal contribution to this work.

<https://doi.org/10.1016/j.bmc.2021.116042>

Received 12 November 2020; Received in revised form 12 January 2021; Accepted 20 January 2021

Available online 2 February 2021

0968-0896/© 2021 Elsevier Ltd. All rights reserved.

It has been previously believed that i-motifs are stable only under acidic conditions *in vitro*,^{25,27–30} while in recent years it has been shown that some genomic C-rich sequences can form stable i-motif structures under neutral conditions *in vitro*.³¹ Besides, molecular crowding conditions can also help to stabilize i-motif structures at physiological pH.³² In addition, metal ions such as Ag⁺ can also stabilize i-motif structures formed in the telomere at pH of 7.4.³³ Recent studies have indicated that i-motif might play important roles in gene regulation, suggesting i-motif as an attractive target for anticancer drug development and gene regulation processes.^{32,34,35} Some i-motifs in oncogenes promoters have been characterized to date,^{34,36–39} including *c-myc*, *bcl2*, PDGFR- β , VEGF, and *n-myc*, and several small molecules have been shown to interact with these i-motif structures as shown in Fig. 1. Ellipticine analog GSA1129 and benzothiothiophene-2-carboxamide (NSC309874) have been found to interact with either G-quadruplex or i-motif in PDGFR- β promoter, resulting in down-regulation of PDGFR- β gene transcription and cancer cells apoptosis.^{37,39}

Previously, we have synthesized and studied an acridone derivative **B19**, which can selectively bind to and stabilize oncogene *c-myc* promoter i-motif, resulting in down-regulation of *c-myc* transcription and translation, however its effect on tumor cells apoptosis requires improvement.⁴⁰ In the present study, we synthesized a variety of **B19** derivatives containing a known anti-cancer fluorescent chromophore naphthalimide for the purpose of enhancing anti-cancer activity. It has been known that naphthalimide chromophore can form stacking interactions with DNA adenine bases⁴¹ with strong anti-cancer properties.^{42–44} Besides, *N*-methylpiperazine group has been shown to interact with G-quadruplex with high affinity in cells,⁴⁵ which was also incorporated into final product. After screening followed with evaluation, we found that acridone-naphthalimide derivative **WZZO2** could bind to both G-quadruplex and i-motif resulting in down-regulation of PDGFR- β gene transcription selectively, with potent anti-cancer activity. **WZZO2** exhibited tumor growth inhibition activity in MCF-7 xenograft tumor model. Our results suggested that **WZZO2** as a dual G-quadruplex/i-motif binder could be effective on both oncogene replication and transcription, and become a promising lead compound for further development with improved potency and selectivity. The wide properties for the derivatives of 1,8-naphthalimide could facilitate further in-depth mechanistic studies of **WZZO2** through various fluorescent physical and chemical methods, which could help to further understand the function of PDGFR- β promoter G-quadruplex and i-motif.

2. Materials and methods

2.1. General method for synthesis

All chemicals were purchased from commercial sources, which were analytical grade without further purification unless otherwise specified. All synthesized compounds were structurally determined by using ¹H, ¹³C NMR spectra and HRMS spectrometry. ¹H and ¹³C NMR spectra were recorded using TMS as the internal standard in CDCl₃ with a Bruker BioSpin GmbH spectrometer at 400 and 100 MHz, respectively. High resolution mass spectra (HRMS) were recorded on Shimadzu LCMS-IT-TOF of MAT95XP mass spectrometer (Thermo Fisher Scientific, USA). The synthetic pathway for methylacridin-9(10H)-one derivatives was shown in Scheme 1.

2.1.1. General procedure for the preparation of compounds L1-L14

To a solution of 4-substituted-1,8-naphthalic anhydride (1.0 mmol) in ethanol (30 mL) was added various alkylamine (3.0 mmol). The reaction mixture was heated under reflux for 20–60 min, and cooled down to room temperature. The solution was concentrated in rotary evaporator and washed with diethyl ether, to give crude yellow solids **L1-L14**. The residue was purified by using chromatograph on silica gel with DCM/MeOH (50/1–30/1) to give desired compounds.

2-(2-aminoethyl)-1H-benzo[de]isoquinoline-1,3(2H)-dione (**L1**). A yellow solid was obtained with a yield of 88%. ¹H NMR (400 MHz, CDCl₃) δ 8.50 (d, *J* = 7.3 Hz, 2H), 8.14 (d, *J* = 8.2 Hz, 2H), 7.67 (t, *J* = 7.8 Hz, 2H), 4.21 (t, *J* = 6.6 Hz, 2H), 3.00 (t, *J* = 6.5 Hz, 2H), 2.42 (s, 2H). ¹³C NMR (101 MHz, CDCl₃) δ 164.49, 134.06, 131.51, 131.28, 128.07, 126.90, 122.36, 42.87, 40.24. ESI-MS *m/z*: 241.45 [M+H]⁺.

2-(3-aminopropyl)-1H-benzo[de]isoquinoline-1,3(2H)-dione (**L2**). A yellow solid was obtained with a yield of 82%. ¹H NMR (400 MHz, CDCl₃) δ 8.55 (dd, *J* = 7.3, 0.9 Hz, 2H), 8.17 (dd, *J* = 8.3, 0.8 Hz, 2H), 7.80–7.62 (m, 2H), 4.25 (t, *J* = 6.9 Hz, 2H), 2.75 (t, *J* = 6.6 Hz, 2H), 1.96–1.81 (m, 2H), 1.49 (s, 2H). ¹³C NMR (101 MHz, CDCl₃) δ 164.26, 133.89, 131.53, 131.20, 128.09, 126.89, 122.55, 39.42, 37.72, 32.12. ESI-MS *m/z*: 255.45 [M+H]⁺.

2-(4-aminobutyl)-1H-benzo[de]isoquinoline-1,3(2H)-dione (**L3**). A yellow solid was obtained with a yield of 80%. ¹H NMR (400 MHz, CDCl₃) δ 8.54 (dd, *J* = 7.3, 1.0 Hz, 2H), 8.15 (dd, *J* = 8.3, 0.9 Hz, 2H), 7.70 (dd, *J* = 11.0, 4.5 Hz, 2H), 4.32–4.05 (m, 2H), 2.74 (t, *J* = 7.0 Hz, 2H), 1.84–1.70 (m, 2H), 1.56 (dd, *J* = 14.9, 7.3 Hz, 2H), 1.48 (s, 2H). ¹³C NMR (101 MHz, CDCl₃) δ 164.15, 133.87, 131.53, 131.16, 128.08, 126.90, 122.62, 41.84, 40.08, 31.12, 25.39. ESI-MS *m/z*: 269.45

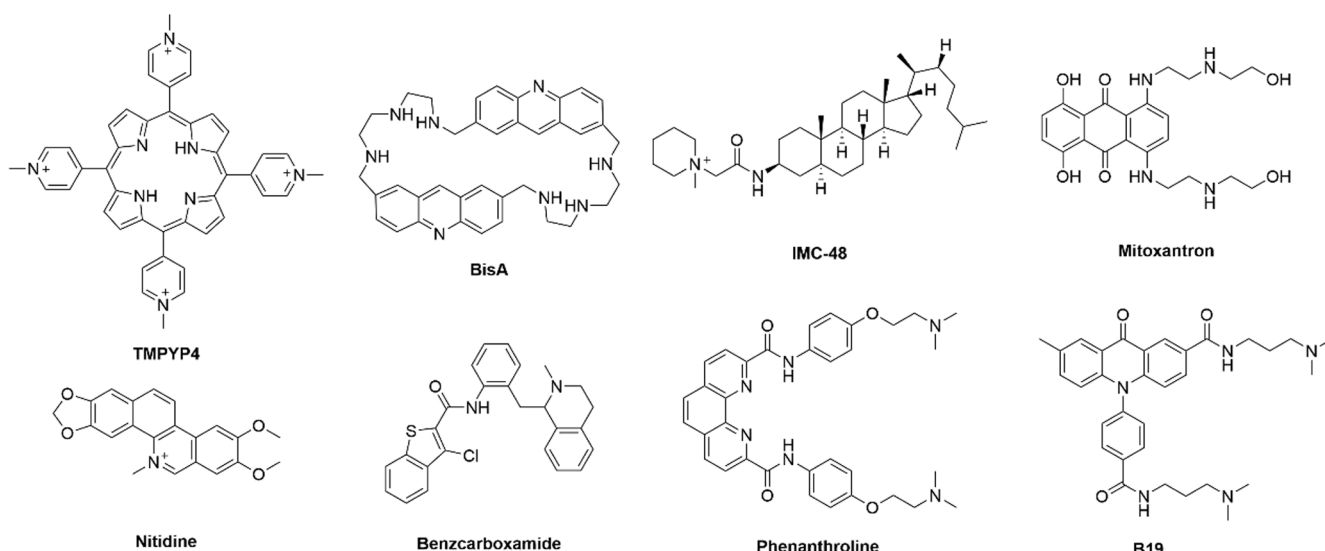
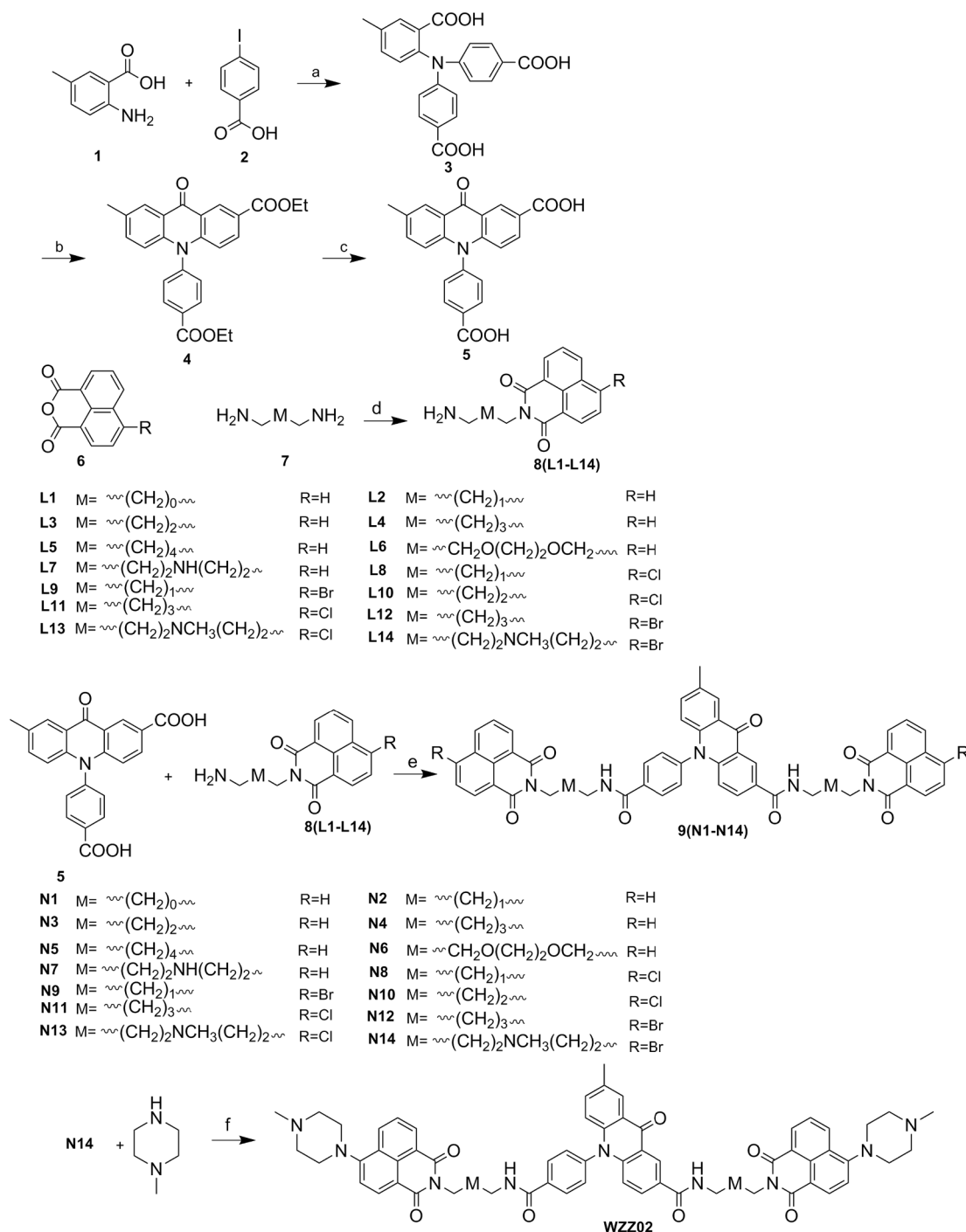


Fig. 1. Structures of TMPYP4, BisA, cholestane (IMC-48), Mitoxantron, Nitidine, Benzcarboxamide, Phenanthroline, and **B19**.



Scheme 1. (a) Cu, CuI, K_2CO_3 , DMF, 120 °C, 24 h; (b) conc. H_2SO_4 , 130 °C, 4 h; EtOH, 80 °C, 2 h (yield, 30% for three steps); (c) MeOH, 10% NaOH, 60 °C, 1 h (yield 91%); (d) EtOH, refluxed, various alkylamine, 20 min-1 h; (e) DCM, EDCI, HOBT, r.t., 4 h; (f) DMF, NaO-*t*-Bu, 5% Pd/C, 1%mol DiCyJohnPhos, 80 °C, 10 h.

$[\text{M}+\text{H}]^+$.

2-(5-aminopentyl)-1H-benzo[de]isoquinoline-1,3(2H)-dione (**L4**). A yellow solid was obtained with a yield of 85%. ^1H NMR (400 MHz, CDCl_3) δ 8.58 (d, $J = 7.3$ Hz, 2H), 8.19 (d, $J = 8.3$ Hz, 2H), 7.73 (t, $J = 7.8$ Hz, 2H), 4.23–4.12 (m, 2H), 2.70 (t, $J = 6.8$ Hz, 2H), 1.74 (dd, $J = 14.9, 7.4$ Hz, 2H), 1.53 (dd, $J = 11.5, 4.7$ Hz, 2H), 1.48 (s, 2H), 1.43 (dd, $J = 9.1, 4.6$ Hz, 2H). ^{13}C NMR (101 MHz, CDCl_3) δ 164.23, 133.91, 131.57, 131.22, 128.14, 126.94, 122.68, 42.09, 40.35, 33.51, 27.97, 24.42. ESI-MS m/z : 283.45 $[\text{M}+\text{H}]^+$.

2-(6-aminohexyl)-1H-benzo[de]isoquinoline-1,3(2H)-dione (**L5**). A yellow solid was obtained with a yield of 78%. ^1H NMR (400 MHz, CDCl_3) δ 8.62–8.50 (m, 2H), 8.16 (d, $J = 5.7$ Hz, 2H), 7.79–7.67 (m, 2H),

4.21–4.08 (m, 2H), 2.65 (d, $J = 6.8$ Hz, 2H), 1.72 (s, 2H), 1.50–1.38 (m, 6H), 1.36 (s, 2H). ^{13}C NMR (101 MHz, CDCl_3) δ 164.18, 133.85, 131.56, 131.16, 128.12, 126.91, 122.71, 42.14, 40.34, 33.71, 28.06, 26.93, 26.56. ESI-MS m/z : 297.50 $[\text{M}+\text{H}]^+$.

2-(2-(2-(2-aminoethoxy)ethoxy)ethyl)-1H-benzo[de]isoquinoline-1,3(2H)-dione (**L6**). A yellow solid was obtained with a yield of 72%. ^1H NMR (400 MHz, CDCl_3) δ 8.54 (dd, $J = 7.3, 0.9$ Hz, 2H), 8.16 (dd, $J = 8.3, 0.8$ Hz, 2H), 7.75–7.67 (m, 2H), 4.41 (t, $J = 6.1$ Hz, 2H), 3.81 (t, $J = 6.1$ Hz, 2H), 3.67 (dd, $J = 5.6, 3.6$ Hz, 2H), 3.56 (dd, $J = 5.7, 3.6$ Hz, 2H), 3.42 (t, $J = 5.2$ Hz, 2H), 2.75 (s, 2H), 1.80 (s, 2H). ^{13}C NMR (101 MHz, CDCl_3) δ 164.21, 134.04, 131.53, 131.24, 128.12, 126.92, 122.52, 73.23, 70.31, 70.08, 67.96, 41.67, 39.08. ESI-MS m/z : 329.45 $[\text{M}+\text{H}]^+$.

2-((3-((3-aminopropyl)amino)propyl)-1H-benzo[de]isoquinoline-1,3(2H)-dione (L7). A yellow solid was obtained with a yield of 68%. ^1H NMR (400 MHz, CDCl_3) δ 8.58 (dd, $J = 7.3, 0.9$ Hz, 2H), 8.25–8.16 (m, 2H), 7.82–7.70 (m, 2H), 4.26 (t, $J = 7.1$ Hz, 2H), 2.78 (t, $J = 6.8$ Hz, 2H), 2.70 (dd, $J = 13.0, 6.7$ Hz, 4H), 2.03–1.90 (m, 2H), 1.72 (s, 3H), 1.70–1.60 (m, 2H). ^{13}C NMR (101 MHz, CDCl_3) δ 164.26, 133.95, 131.55, 131.23, 128.11, 126.93, 122.58, 47.65, 47.16, 40.47, 38.29, 33.73, 28.34. ESI-MS m/z : 312.50 $[\text{M}+\text{H}]^+$.

2-(3-aminopropyl)-6-chloro-1H-benzo[de]isoquinoline-1,3(2H)-dione (L8). A yellow solid was obtained with a yield of 75%. ^1H NMR (400 MHz, CDCl_3) δ 8.48 (d, $J = 7.0$ Hz, 1H), 8.39 (d, $J = 8.3$ Hz, 1H), 8.31 (d, $J = 7.8$ Hz, 1H), 7.74–7.60 (m, 2H), 4.16 (t, $J = 6.9$ Hz, 2H), 2.70 (t, $J = 6.5$ Hz, 2H), 1.88–1.74 (m, 2H), 1.43 (s, 2H). ^{13}C NMR (101 MHz, CDCl_3) δ 163.59, 163.33, 138.85, 131.85, 130.95, 130.41, 128.99, 128.73, 127.71, 127.22, 122.75, 121.29, 39.40, 37.83, 32.02. ESI-MS m/z : 289.25 $[\text{M}+\text{H}]^+$.

2-(3-aminopropyl)-6-bromo-1H-benzo[de]isoquinoline-1,3(2H)-dione (L9). A yellow solid was obtained with a yield of 73%. ^1H NMR (400 MHz, CDCl_3) δ 8.68–8.61 (m, 1H), 8.55 (d, $J = 8.5$ Hz, 1H), 8.39 (d, $J = 7.9$ Hz, 1H), 8.02 (d, $J = 7.9$ Hz, 1H), 7.83 (dd, $J = 8.4, 7.5$ Hz, 1H), 4.26 (t, $J = 6.9$ Hz, 2H), 2.77 (s, 2H), 1.99–1.80 (m, 2H), 1.49 (s, 2H). ^{13}C NMR (101 MHz, CDCl_3) δ 163.77, 163.74, 133.35, 132.12, 131.30, 131.13, 130.63, 130.36, 128.99, 128.11, 122.99, 122.12, 39.38, 37.90, 32.04. ESI-MS m/z : 334.30 $[\text{M}+\text{H}]^+$.

2-(4-aminobutyl)-6-chloro-1H-benzo[de]isoquinoline-1,3(2H)-dione (L10). A yellow solid was obtained with a yield of 63%. ^1H NMR (400 MHz, CDCl_3) δ 8.59 (d, $J = 7.2$ Hz, 1H), 8.52 (d, $J = 8.3$ Hz, 1H), 8.43 (d, $J = 7.9$ Hz, 1H), 7.85–7.72 (m, 2H), 4.22–4.07 (m, 2H), 2.75 (t, $J = 6.9$ Hz, 2H), 1.74 (dd, $J = 15.2, 7.8$ Hz, 4H), 1.56 (dd, $J = 14.9, 7.3$ Hz, 2H). ^{13}C NMR (101 MHz, CDCl_3) δ 163.68, 163.42, 139.00, 131.97, 131.08, 130.59, 129.22, 128.96, 127.82, 127.34, 122.98, 121.48, 41.75, 40.20, 31.02, 25.34. ESI-MS m/z : 303.95 $[\text{M}+\text{H}]^+$.

2-(5-aminopentyl)-6-chloro-1H-benzo[de]isoquinoline-1,3(2H)-dione (L11). A yellow solid was obtained with a yield of 65%. ^1H NMR (400 MHz, CDCl_3) δ 8.59 (d, $J = 7.2$ Hz, 1H), 8.50 (d, $J = 8.5$ Hz, 1H), 8.35 (d, $J = 7.9$ Hz, 1H), 7.98 (d, $J = 7.9$ Hz, 1H), 7.80 (t, $J = 7.9$ Hz, 1H), 4.19–4.07 (m, 2H), 2.70 (t, $J = 6.8$ Hz, 2H), 1.83 (s, 2H), 1.73 (dt, $J = 14.9, 7.5$ Hz, 2H), 1.57–1.48 (m, 2H), 1.48–1.38 (m, 2H). ^{13}C NMR (101 MHz, CDCl_3) δ 163.57 (s), 163.55 (s), 133.20 (s), 131.99 (s), 131.17 (s), 131.06 (s), 130.54 (s), 130.21 (s), 128.90 (s), 128.05 (s), 123.02 (s), 122.15 (s), 41.93 (s), 40.44 (s), 33.18 (s), 27.86 (s), 24.36 (s). ESI-MS m/z : 317.35 $[\text{M}+\text{H}]^+$.

2-(5-aminopentyl)-6-bromo-1H-benzo[de]isoquinoline-1,3(2H)-dione (L12). A yellow solid was obtained with a yield of 71%. ^1H NMR (400 MHz, CDCl_3) δ 8.59 (d, $J = 7.2$ Hz, 1H), 8.50 (d, $J = 8.5$ Hz, 1H), 8.35 (d, $J = 7.9$ Hz, 1H), 7.98 (d, $J = 7.9$ Hz, 1H), 7.80 (t, $J = 7.9$ Hz, 1H), 4.19–4.07 (m, 2H), 2.70 (t, $J = 6.8$ Hz, 2H), 1.73 (dt, $J = 14.9, 7.5$ Hz, 2H), 1.57–1.48 (m, 2H), 1.48–1.38 (m, 2H). ^{13}C NMR (101 MHz, CDCl_3) δ 163.57, 163.55, 133.20, 131.99, 131.17, 131.06, 130.54, 130.21, 128.90, 128.05, 41.93, 40.44, 33.18, 27.86, 24.36. ESI-MS m/z : 362.35 $[\text{M}+\text{H}]^+$.

2-((3-((3-aminopropyl)(methyl)amino)propyl)-6-chloro-1H-benzo[de]isoquinoline-1,3(2H)-dione (L13). A yellow solid was obtained with a yield of 65%. ^1H NMR (400 MHz, CDCl_3) δ 8.60 (d, $J = 7.2$ Hz, 1H), 8.52 (d, $J = 8.5$ Hz, 1H), 8.43 (d, $J = 7.9$ Hz, 1H), 7.79 (dd, $J = 17.6, 8.0$ Hz, 2H), 4.24–4.12 (m, 2H), 3.16 (s, 2H), 2.96–2.82 (m, 2H), 2.46 (dd, $J = 13.7, 6.8$ Hz, 4H), 2.24 (s, 3H), 1.95–1.82 (m, 2H), 1.77–1.63 (m, 2H). ^{13}C NMR (101 MHz, CDCl_3) δ 163.68, 163.43, 139.04, 132.02, 131.14, 130.60, 129.21, 128.95, 127.82, 127.35, 122.94, 121.45, 55.98, 55.57, 41.82, 40.73, 38.86, 28.38, 25.62. ESI-MS m/z : 360.10 $[\text{M}+\text{H}]^+$.

2-((3-((3-aminopropyl)(methyl)amino)propyl)-6-bromo-1H-benzo[de]isoquinoline-1,3(2H)-dione (L14). A yellow solid was obtained with a yield of 61%. ^1H NMR (400 MHz, CDCl_3) δ 8.63 (d, $J = 7.2$ Hz, 1H), 8.54 (d, $J = 8.5$ Hz, 1H), 8.39 (d, $J = 7.9$ Hz, 1H), 8.02 (d, $J = 7.9$ Hz, 1H), 7.83 (t, $J = 7.9$ Hz, 1H), 4.26–4.17 (m, 2H), 2.84 (t, $J = 6.5$ Hz, 2H), 2.55 (s, 2H), 2.51–2.48 (m, 2H), 2.45 (t, $J = 6.9$ Hz, 2H), 2.26 (s, 3H),

1.96–1.85 (m, 2H), 1.75–1.62 (m, 2H). ^{13}C NMR (101 MHz, CDCl_3) δ 163.48, 163.44, 133.16, 131.99, 131.16, 131.02, 130.36, 130.25, 128.68, 128.01, 122.75, 121.89, 56.15, 55.55, 41.78, 40.80, 38.80, 27.50, 25.54. ESI-MS m/z : 404.30 $[\text{M}+\text{H}]^+$.

2.1.2. General procedure for the preparation of compounds N1–N14

To a solution of 10-(4-carboxyphenyl)-7-methyl-9-oxo-9,10-dihydroacridine-2-carboxylic acid (5) (0.16 mmol) and L(1–14) (0.48 mmol) in anhydrous dichloromethane (15 mL) was added 1-(3-dimethylaminopropyl)-3-ethylcarbodiimide hydrochloride (EDCI) (0.48 mmol), and then 1-hydroxybenzotriazole (HOBT) (0.48 mmol). The reaction mixture was stirred at room temperature under nitrogen atmosphere for 6 h. The reaction mixture was quenched with 10 mL ice water, and the filtrate was extracted with dichloromethane (3×10 mL). The combined organic layer was washed with brine, dried over anhydrous sodium sulfate, filtered, and then concentrated under reduced pressure to give crude yellow solids N(1–14). The residue was purified by using chromatograph on silica gel with DCM/MeOH (50/1–10/1) to give desired compounds.

N-(2-(1,3-dioxo-1H-benzo[de]isoquinolin-2(3H)-yl)ethyl)-10-(4-((2-(1,3-dioxo-1H-benzo[de]isoquinolin-2(3H)-yl)ethyl)carbamoyl)phenyl)-7-methyl-9-oxo-9,10-dihydroacridine-2-carboxamide (N1). A yellow solid was obtained with a yield of 78%. ^1H NMR (400 MHz, CDCl_3) δ 8.68 (d, $J = 2.0$ Hz, 1H), 8.61–8.47 (m, 4H), 8.21–8.05 (m, 7H), 7.84 (dd, $J = 9.0, 2.1$ Hz, 1H), 7.81–7.51 (m, 6H), 7.30 (d, $J = 8.3$ Hz, 2H), 7.22 (dd, $J = 8.8, 2.0$ Hz, 1H), 6.51 (dd, $J = 14.3, 8.8$ Hz, 2H), 4.68–4.37 (m, 4H), 4.12–3.78 (m, 4H), 2.37 (s, 3H). ^{13}C NMR (101 MHz, CDCl_3) δ 177.45, 166.69, 166.44, 165.11, 164.83, 143.92, 140.96, 140.64, 136.00, 135.12, 134.33, 134.03, 132.48, 132.09, 131.54, 131.46, 131.38, 130.06, 130.01, 128.08, 128.07, 127.28, 126.96, 126.91, 126.40, 125.62, 122.30, 122.17, 121.45, 120.33, 116.76, 100.00, 40.46, 39.81, 39.66, 20.67. HRMS (ESI; m/z). Calcd for C50H35N5O7, $[\text{M}+\text{H}]^+$, 818.2609; found, 818.2608.

N-(3-(1,3-dioxo-1H-benzo[de]isoquinolin-2(3H)-yl)propyl)-10-(4-((3-(1,3-dioxo-1H-benzo[de]isoquinolin-2(3H)-yl)propyl)carbamoyl)phenyl)-7-methyl-9-oxo-9,10-dihydroacridine-2-carboxamide (N2). A yellow solid was obtained with a yield of 68%. ^1H NMR (400 MHz, CDCl_3) δ 9.12 (d, $J = 2.1$ Hz, 1H), 8.73–8.61 (m, 4H), 8.40 (d, $J = 1.0$ Hz, 1H), 8.34 (d, $J = 8.4$ Hz, 2H), 8.29–8.20 (m, 4H), 8.15 (dd, $J = 9.0, 2.2$ Hz, 1H), 7.78 (dd, $J = 15.7, 8.3$ Hz, 5H), 7.64 (t, $J = 5.9$ Hz, 1H), 7.53 (d, $J = 8.4$ Hz, 2H), 7.37 (dd, $J = 8.8, 2.0$ Hz, 1H), 6.84 (d, $J = 9.0$ Hz, 1H), 6.71 (d, $J = 8.7$ Hz, 1H), 4.39 (dt, $J = 15.4, 6.2$ Hz, 4H), 3.55 (td, $J = 11.8, 6.0$ Hz, 4H), 2.48 (s, 3H), 2.21–2.06 (m, 4H). ^{13}C NMR (101 MHz, CDCl_3) δ 177.88, 166.25, 165.91, 165.01, 164.79, 144.30, 141.31, 140.99, 136.30, 135.24, 134.55, 134.25, 132.63, 132.29, 131.76, 131.65, 131.59, 130.34, 130.13, 128.22, 127.66, 127.14, 127.07, 126.75, 125.76, 122.37, 122.24, 121.92, 120.87, 117.05, 116.95, 37.70, 37.58, 36.68, 36.44, 27.97, 27.86, 20.76. HRMS (ESI; m/z). Calcd for C52H39N5O7, $[\text{M}+\text{H}]^+$, 846.2922; found, 846.2925.

N-(4-(1,3-dioxo-1H-benzo[de]isoquinolin-2(3H)-yl)butyl)-10-(4-((4-(1,3-dioxo-1H-benzo[de]isoquinolin-2(3H)-yl)butyl)carbamoyl)phenyl)-7-methyl-9-oxo-9,10-dihydroacridine-2-carboxamide (N3). A yellow solid was obtained with a yield of 58%. ^1H NMR (400 MHz, CDCl_3) δ 8.86 (s, 1H), 8.55 (dd, $J = 14.0, 7.3$ Hz, 4H), 8.23 (d, $J = 9.9$ Hz, 2H), 8.19 (d, $J = 5.0$ Hz, 2H), 8.15 (d, $J = 7.7$ Hz, 3H), 8.02 (d, $J = 8.8$ Hz, 1H), 7.70 (t, $J = 7.7$ Hz, 4H), 7.39 (d, $J = 8.1$ Hz, 2H), 7.29 (s, 1H), 7.23 (s, 1H), 7.09 (s, 1H), 6.70 (d, $J = 9.0$ Hz, 1H), 6.60 (d, $J = 8.7$ Hz, 1H), 4.23 (d, $J = 7.0$ Hz, 4H), 3.67 (d, $J = 5.9$ Hz, 2H), 3.58 (d, $J = 6.0$ Hz, 2H), 2.41 (s, 3H), 1.93–1.76 (m, 8H). ^{13}C NMR (101 MHz, CDCl_3) δ 177.82, 166.30, 164.41, 164.34, 144.19, 141.10, 140.92, 136.36, 135.29, 134.23, 134.00, 132.94, 132.30, 131.60, 131.56, 131.46, 131.35, 130.13, 128.16, 128.13, 127.48, 127.03, 126.97, 126.61, 125.22, 122.58, 122.48, 121.77, 120.57, 117.02, 116.91, 39.65, 39.56, 39.52, 26.77, 26.28, 25.58, 25.44, 20.72. HRMS (ESI; m/z). Calcd for C54H43N5O7, $[\text{M}+\text{H}]^+$, 874.3235; found, 874.3239.

N-(5-(1,3-dioxo-1H-benzo[de]isoquinolin-2(3H)-yl)pentyl)-10-(4-

((5-(1,3-dioxo-1H-benzo[de]isoquinolin-2(3H)-yl)pentyl)carbamoyl)phenyl)-7-methyl-9-oxo-9,10-dihydroacridine-2-carboxamide (**N4**). A yellow solid was obtained with a yield of 53%. ^1H NMR (400 MHz, CDCl_3) δ 8.85 (s, 1H), 8.56 (d, $J = 7.2$ Hz, 4H), 8.32 (s, 1H), 8.19 (s, 1H), 8.17 (s, 3H), 8.15 (s, 2H), 8.03 (s, 1H), 7.69 (t, $J = 7.7$ Hz, 4H), 7.41 (d, $J = 8.2$ Hz, 2H), 7.33 (d, $J = 8.8$ Hz, 1H), 6.73 (d, $J = 8.8$ Hz, 3H), 6.63 (d, $J = 8.7$ Hz, 1H), 4.24–4.15 (m, 4H), 3.55 (dd, $J = 23.9, 6.0$ Hz, 4H), 2.45 (s, 3H), 1.87–1.74 (m, 12H). ^{13}C NMR (101 MHz, CDCl_3) δ 177.79, 166.41, 166.36, 164.44, 164.29, 144.15, 141.06, 140.90, 136.50, 135.35, 134.11, 133.89, 132.92, 132.37, 131.58, 131.53, 131.27, 130.14, 130.11, 128.12, 127.61, 126.96, 126.91, 126.65, 125.15, 122.63, 122.55, 121.75, 120.55, 117.00, 116.89, 40.30, 40.13, 40.06, 39.96, 29.20, 28.85, 27.79, 27.76, 24.46, 24.37, 20.73. HRMS (ESI; m/z). Calcd for $\text{C}_{56}\text{H}_{47}\text{N}_5\text{O}_7$, $[\text{M}+\text{H}]^+$, 902.3548; found, 902.3553.

N-(6-(1,3-dioxo-1H-benzo[de]isoquinolin-2(3H)-yl)hexyl)-10-(4-((6-(1,3-dioxo-1H-benzo[de]isoquinolin-2(3H)-yl)hexyl)carbamoyl)phenyl)-7-methyl-9-oxo-9,10-dihydroacridine-2-carboxamide (**N5**). A yellow solid was obtained with a yield of 62%. ^1H NMR (400 MHz, CDCl_3) δ 8.84 (s, 1H), 8.65–8.47 (m, 4H), 8.28 (s, 1H), 8.27–8.11 (m, 6H), 8.05 (d, $J = 7.3$ Hz, 1H), 7.72 (t, $J = 7.5$ Hz, 4H), 7.42 (d, $J = 6.5$ Hz, 2H), 7.30 (d, $J = 8.3$ Hz, 1H), 6.81 (s, 1H), 6.74 (s, 2H), 6.62 (d, $J = 8.5$ Hz, 1H), 4.18 (dd, $J = 14.9, 7.9$ Hz, 4H), 3.51 (d, $J = 25.2$ Hz, 4H), 2.42 (s, 3H), 1.84–1.64 (m, 8H), 1.49 (s, 8H). ^{13}C NMR (101 MHz, CDCl_3) δ 177.77, 166.37, 166.32, 164.31, 164.23, 144.12, 141.04, 140.87, 136.50, 135.28, 134.03, 133.87, 132.83, 132.27, 131.56, 131.54, 131.21, 130.14, 130.11, 128.10, 127.62, 126.96, 126.92, 126.57, 125.15, 122.65, 122.57, 121.72, 120.55, 117.02, 116.87, 40.11, 40.01, 29.47, 29.28, 27.91, 27.83, 26.54, 26.50, 26.35, 26.27, 20.70. HRMS (ESI; m/z). Calcd for $\text{C}_{58}\text{H}_{51}\text{N}_5\text{O}_7$, $[\text{M}+\text{H}]^+$, 930.3861; found, 930.3863.

N-(2-(2-(2-(1,3-dioxo-1H-benzo[de]isoquinolin-2(3H)-yl)ethoxy)ethoxy)ethyl)carbamoyl)phenyl)-7-methyl-9-oxo-9,10-dihydroacridine-2-carboxamide (**N6**). A yellow solid was obtained with a yield of 56%. ^1H NMR (400 MHz, CDCl_3) δ 8.85 (s, 1H), 8.46 (dd, $J = 9.8, 7.5$ Hz, 4H), 8.27–8.07 (m, 8H), 7.97 (d, $J = 8.9$ Hz, 1H), 7.64 (dd, $J = 16.4, 8.2$ Hz, 4H), 7.37 (d, $J = 8.1$ Hz, 3H), 7.28 (s, 1H), 6.68 (d, $J = 9.0$ Hz, 1H), 6.57 (d, $J = 8.7$ Hz, 1H), 4.45 (q, $J = 5.6$ Hz, 4H), 3.91 (t, $J = 5.8$ Hz, 2H), 3.86 (t, $J = 6.0$ Hz, 2H), 3.74 (d, $J = 4.2$ Hz, 4H), 3.66 (d, $J = 13.6$ Hz, 10H), 3.64–3.58 (m, 2H), 2.40 (s, 3H). ^{13}C NMR (101 MHz, CDCl_3) δ 177.61, 166.45, 166.22, 164.33, 164.29, 144.05, 141.13, 140.80, 136.12, 135.11, 134.24, 133.83, 132.54, 132.11, 131.55, 131.44, 131.30, 131.15, 130.18, 130.12, 128.08, 127.47, 126.96, 126.81, 126.61, 125.74, 122.53, 122.32, 121.72, 120.59, 116.84, 116.78, 70.52, 70.28, 70.17, 70.14, 69.78, 69.68, 68.30, 68.11, 40.06, 39.97, 39.28, 39.22, 20.67. HRMS (ESI; m/z). Calcd for $\text{C}_{58}\text{H}_{51}\text{N}_5\text{O}_{11}$, $[\text{M}+\text{H}]^+$, 994.3658; found, 994.3682.

N-(3-(3-(1,3-dioxo-1H-benzo[de]isoquinolin-2(3H)-yl)propyl)amino)propyl)-10-(4-((3-(3-(1,3-dioxo-1H-benzo[de]isoquinolin-2(3H)-yl)propyl)amino)propyl)carbamoyl)phenyl)-7-methyl-9-oxo-9,10-dihydroacridine-2-carboxamide (**N7**). A yellow solid was obtained with a yield of 66%. ^1H NMR (400 MHz, CDCl_3) δ 8.97 (s, 1H), 8.83 (d, $J = 2.1$ Hz, 1H), 8.46 (d, $J = 7.1$ Hz, 2H), 8.37 (t, $J = 9.0$ Hz, 3H), 8.18 (d, $J = 8.3$ Hz, 2H), 8.11 (d, $J = 7.8$ Hz, 4H), 8.00 (d, $J = 9.2$ Hz, 2H), 7.64 (t, $J = 7.8$ Hz, 2H), 7.56 (t, $J = 7.7$ Hz, 2H), 7.37 (d, $J = 8.2$ Hz, 2H), 7.16 (d, $J = 8.8$ Hz, 1H), 6.70 (d, $J = 9.0$ Hz, 1H), 6.50 (d, $J = 8.8$ Hz, 1H), 4.25 (t, $J = 5.8$ Hz, 5H), 3.74–3.57 (m, 5H), 2.94 (d, $J = 5.7$ Hz, 2H), 2.87 (d, $J = 6.0$ Hz, 2H), 2.79 (q, $J = 6.5$ Hz, 4H), 2.27 (s, 3H), 2.11–2.02 (m, 2H), 2.03–1.95 (m, 2H), 1.88 (d, $J = 4.9$ Hz, 4H). ^{13}C NMR (101 MHz, CDCl_3) δ 177.61, 166.45, 166.22, 164.33, 164.29, 144.05, 141.13, 140.80, 136.12, 135.11, 134.24, 133.83, 132.54, 132.11, 131.55, 131.44, 131.30, 131.15, 130.18, 130.12, 128.08, 127.47, 126.96, 126.81, 126.61, 125.74, 122.53, 122.32, 121.72, 120.59, 116.84, 116.78, 70.52, 70.28, 70.17, 70.14, 69.78, 69.68, 68.30, 68.11, 40.06, 39.97, 39.28, 39.22, 20.67. HRMS (ESI; m/z). Calcd for $\text{C}_{58}\text{H}_{53}\text{N}_7\text{O}_7$, $[\text{M}+2\text{H}]^{2+}$, 480.7076; found, 480.7063.

N-(3-(6-chloro-1,3-dioxo-1H-benzo[de]isoquinolin-2(3H)-yl)propyl)-10-(4-((3-(6-chloro-1,3-dioxo-1H-benzo[de]isoquinolin-2(3H)-yl)propyl)carbamoyl)phenyl)-7-methyl-9-oxo-9,10-dihydroacridine-2-carboxamide (**N8**). A yellow solid was obtained with a yield of 62%. ^1H NMR (400 MHz, CDCl_3) δ 9.06 (d, $J = 2.0$ Hz, 1H), 8.71 (dd, $J = 7.0, 4.6$ Hz, 2H), 8.63 (d, $J = 8.3$ Hz, 1H), 8.60–8.52 (m, 3H), 8.38–8.30 (m, 3H), 8.12 (dd, $J = 9.1, 2.0$ Hz, 1H), 7.92–7.79 (m, 4H), 7.75 (t, $J = 6.1$ Hz, 1H), 7.60 (t, $J = 6.0$ Hz, 1H), 7.54 (d, $J = 8.3$ Hz, 2H), 7.36 (dd, $J = 8.8, 2.0$ Hz, 1H), 6.82 (d, $J = 9.0$ Hz, 1H), 6.69 (d, $J = 8.7$ Hz, 1H), 4.41–4.30 (m, 4H), 3.59–3.49 (m, 4H), 2.47 (s, 3H), 2.12 (dd, $J = 12.7, 6.2$ Hz, 4H). ^{13}C NMR (101 MHz, CDCl_3) δ 177.81, 166.23, 165.94, 164.51, 164.26, 164.04, 144.26, 141.31, 140.96, 139.75, 139.39, 136.26, 135.26, 132.64, 132.51, 132.31, 131.63, 131.24, 130.92, 130.35, 130.12, 129.41, 129.29, 129.12, 129.09, 128.03, 127.96, 127.57, 127.54, 127.49, 126.72, 125.63, 122.76, 122.64, 121.87, 121.25, 121.10, 120.78, 117.02, 116.94, 37.89, 37.71, 36.79, 36.46, 27.91, 27.83, 20.76. HRMS (ESI; m/z). Calcd for $\text{C}_{52}\text{H}_{37}\text{N}_5\text{O}_7\text{Cl}_2$, $[\text{M}+\text{H}]^+$, 914.2143; found, 914.2163.

N-(3-(6-bromo-1,3-dioxo-1H-benzo[de]isoquinolin-2(3H)-yl)propyl)-10-(4-((3-(6-bromo-1,3-dioxo-1H-benzo[de]isoquinolin-2(3H)-yl)propyl)carbamoyl)phenyl)-7-methyl-9-oxo-9,10-dihydroacridine-2-carboxamide (**N9**). A yellow solid was obtained with a yield of 50%. ^1H NMR (400 MHz, CDCl_3) δ 9.03 (d, $J = 1.8$ Hz, 1H), 8.67 (t, $J = 5.7$ Hz, 2H), 8.58 (dd, $J = 8.0, 4.1$ Hz, 1H), 8.52 (t, $J = 6.8$ Hz, 1H), 8.46–8.38 (m, 2H), 8.33 (d, $J = 8.1$ Hz, 3H), 8.09 (d, $J = 8.9$ Hz, 1H), 8.06–7.96 (m, 2H), 7.89–7.74 (m, 3H), 7.61 (s, 1H), 7.54 (d, $J = 8.1$ Hz, 2H), 7.35 (d, $J = 8.7$ Hz, 1H), 6.80 (d, $J = 8.9$ Hz, 1H), 6.68 (d, $J = 8.7$ Hz, 1H), 4.34 (dd, $J = 13.0, 6.3$ Hz, 4H), 3.53 (s, 4H), 2.45 (s, 3H), 2.13 (d, $J = 6.3$ Hz, 2H), 2.10 (d, $J = 6.1$ Hz, 2H). ^{13}C NMR (101 MHz, CDCl_3) δ 177.75, 166.25, 165.96, 164.34, 164.11, 144.22, 141.28, 140.93, 136.25, 135.25, 133.85, 133.51, 132.60, 132.49, 132.28, 131.66, 131.27, 131.19, 130.98, 130.70, 130.61, 130.56, 130.34, 130.13, 129.00, 128.96, 128.24, 128.17, 127.50, 126.67, 125.64, 122.74, 122.63, 121.86, 121.81, 121.73, 120.72, 117.00, 116.94, 37.93, 37.75, 36.83, 36.52, 27.91, 27.83, 20.76. HRMS (ESI; m/z). Calcd for $\text{C}_{52}\text{H}_{37}\text{N}_5\text{O}_7\text{Br}_2$, $[\text{M}+\text{H}]^+$, 1002.1132; found, 1002.1093.

N-(4-(6-chloro-1,3-dioxo-1H-benzo[de]isoquinolin-2(3H)-yl)butyl)-10-(4-((4-(6-chloro-1,3-dioxo-1H-benzo[de]isoquinolin-2(3H)-yl)butyl)carbamoyl)phenyl)-7-methyl-9-oxo-9,10-dihydroacridine-2-carboxamide (**N10**). A yellow solid was obtained with a yield of 60%. ^1H NMR (400 MHz, CDCl_3) δ 8.90 (d, $J = 2.0$ Hz, 1H), 8.70 (d, $J = 7.3$ Hz, 1H), 8.65 (d, $J = 7.2$ Hz, 1H), 8.63–8.53 (m, 3H), 8.49 (d, $J = 7.9$ Hz, 1H), 8.34 (s, 1H), 8.19 (d, $J = 8.3$ Hz, 2H), 8.09 (dd, $J = 9.0, 2.0$ Hz, 1H), 7.84 (dd, $J = 16.3, 8.2$ Hz, 4H), 7.43 (d, $J = 8.3$ Hz, 2H), 7.34 (d, $J = 8.7$ Hz, 1H), 7.01–6.86 (m, 2H), 6.76 (d, $J = 9.0$ Hz, 1H), 6.64 (d, $J = 8.7$ Hz, 1H), 4.26 (dd, $J = 13.9, 6.5$ Hz, 4H), 3.65 (dd, $J = 30.4, 6.1$ Hz, 4H), 2.46 (s, 3H), 1.86 (ddd, $J = 31.3, 16.6, 7.9$ Hz, 8H). ^{13}C NMR (101 MHz, CDCl_3) δ 177.72, 166.31, 163.90, 163.83, 163.63, 163.58, 144.12, 141.06, 140.85, 139.31, 139.07, 136.33, 135.29, 132.90, 132.30, 132.21, 132.10, 131.34, 131.21, 130.85, 130.64, 130.12, 130.10, 129.29, 129.23, 129.02, 129.00, 127.89, 127.85, 127.45, 127.42, 127.38, 126.53, 125.18, 122.94, 122.86, 121.68, 121.45, 121.35, 120.51, 116.97, 116.89, 39.76, 39.67, 39.60, 26.78, 26.47, 25.54, 25.49, 20.72. HRMS (ESI; m/z). Calcd for $\text{C}_{54}\text{H}_{41}\text{N}_5\text{O}_7\text{Cl}_2$, $[\text{M}+\text{H}]^+$, 942.2456; found, 942.2473.

N-(5-(6-chloro-1,3-dioxo-1H-benzo[de]isoquinolin-2(3H)-yl)pentyl)-10-(4-((5-(6-chloro-1,3-dioxo-1H-benzo[de]isoquinolin-2(3H)-yl)pentyl)carbamoyl)phenyl)-7-methyl-9-oxo-9,10-dihydroacridine-2-carboxamide (**N11**). A yellow solid was obtained with a yield of 40%. ^1H NMR (400 MHz, CDCl_3) δ 8.72 (s, 1H), 8.49 (s, 2H), 8.44 (d, $J = 8.2$ Hz, 1H), 8.39 (d, $J = 7.9$ Hz, 1H), 8.35–8.28 (m, 2H), 8.19–8.04 (m, 3H), 7.92 (d, $J = 6.4$ Hz, 1H), 7.67 (ddd, $J = 12.5, 10.7, 5.7$ Hz, 4H), 7.32 (d, $J = 5.7$ Hz, 2H), 7.23 (s, 1H), 7.05 (d, $J = 47.2$ Hz, 2H), 6.61 (d, $J = 6.7$ Hz, 1H), 6.52 (d, $J = 7.9$ Hz, 1H), 4.13 (d, $J = 5.9$ Hz, 4H), 3.65–3.41 (m, 4H), 2.36 (s, 3H), 1.78 (s, 8H), 1.60–1.48 (m, 4H). ^{13}C NMR (101 MHz, CDCl_3) δ 177.53, 166.55, 166.35, 163.77, 163.69, 163.51, 163.44,

143.94, 140.90, 140.72, 139.00, 138.81, 136.42, 135.28, 132.73, 132.22, 131.90, 131.01, 130.56, 130.37, 130.16, 129.99, 129.11, 129.04, 128.85, 127.75, 127.70, 127.60, 127.26, 127.22, 126.41, 125.24, 122.89, 122.85, 121.51, 121.40, 121.36, 120.38, 116.83, 40.20, 40.12, 29.15, 29.10, 27.75, 24.46, 20.69. HRMS (ESI; m/z). Calcd for C₅₆H₄₅N₅O₇Cl₂, [M+H]⁺, 970.2769; found, 970.2763.

N-(5-(6-bromo-1,3-dioxo-1H-benzo[de]isoquinolin-2(3H)-yl)pentyl)-10-(4-((5-(6-bromo-1,3-dioxo-1H-benzo[de]isoquinolin-2(3H)-yl)pentyl)carbamoyl)phenyl)-7-methyl-9-oxo-9,10-dihydroacridine-2-carboxamide (N12). A yellow solid was obtained with a yield of 45%. ¹H NMR (400 MHz, CDCl₃) δ 8.79 (d, J = 2.1 Hz, 1H), 8.59 (dd, J = 6.8, 2.2 Hz, 2H), 8.55–8.43 (m, 2H), 8.34 (dd, J = 7.8, 1.3 Hz, 2H), 8.25 (s, 1H), 8.13 (d, J = 8.3 Hz, 2H), 8.06–7.98 (m, 1H), 7.94 (t, J = 7.5 Hz, 2H), 7.76 (dd, J = 15.8, 7.4 Hz, 2H), 7.38 (d, J = 8.2 Hz, 2H), 7.31 (dd, J = 8.8, 2.0 Hz, 1H), 6.85–6.72 (m, 2H), 6.69 (d, J = 9.0 Hz, 1H), 6.60 (d, J = 8.7 Hz, 1H), 4.19 (dd, J = 14.2, 6.9 Hz, 4H), 3.61–3.45 (m, 4H), 2.44 (s, 3H), 1.84–1.77 (m, 8H), 1.57 (dd, J = 15.6, 7.4 Hz, 4H). ¹³C NMR (101 MHz, CDCl₃) δ 177.63, 166.51, 166.38, 163.73, 163.71, 163.64, 163.63, 144.01, 140.94, 140.78, 136.45, 135.35, 133.28, 133.09, 132.81, 132.31, 132.00, 131.19, 131.16, 131.03, 130.99, 130.51, 130.43, 130.34, 130.13, 130.03, 128.84, 128.02, 127.98, 127.59, 126.48, 125.18, 122.95, 122.91, 122.09, 122.04, 121.58, 120.42, 116.90, 116.85, 40.21, 40.09, 29.14, 29.04, 27.73, 24.42, 20.72. HRMS (ESI; m/z). Calcd for C₅₆H₄₅N₅O₇Br₂, [M+H]⁺, 1058.1758; found, 1058.1685.

N-(3-((3-(6-chloro-1,3-dioxo-1H-benzo[de]isoquinolin-2(3H)-yl)propyl)(methyl)amino)propyl)-10-(4-((3-((3-(6-chloro-1,3-dioxo-1H-benzo[de]isoquinolin-2(3H)-yl)propyl)(methyl)amino)propyl)carbamoyl)phenyl)-7-methyl-9-oxo-9,10-dihydroacridine-2-carboxamide (N13). A yellow solid was obtained with a yield of 42%. ¹H NMR (400 MHz, CDCl₃) δ 8.70 (d, J = 1.9 Hz, 1H), 8.69–8.57 (m, 2H), 8.47–8.39 (m, 2H), 8.36 (d, J = 7.1 Hz, 1H), 8.29 (dd, J = 16.6, 8.1 Hz, 2H), 8.18 (d, J = 7.8 Hz, 3H), 7.95 (dd, J = 8.8, 1.9 Hz, 1H), 7.63 (dd, J = 14.4, 7.3 Hz, 4H), 7.56 (d, J = 7.9 Hz, 1H), 7.35 (d, J = 7.2 Hz, 2H), 7.08 (d, J = 8.8 Hz, 1H), 6.66 (d, J = 8.8 Hz, 1H), 6.43 (d, J = 8.5 Hz, 1H), 4.27–4.11 (m, 4H), 3.75–3.59 (m, 4H), 2.67 (s, 8H), 2.43 (d, J = 11.9 Hz, 6H), 2.22 (s, 3H), 2.06 (dd, J = 13.0, 5.5 Hz, 2H), 2.03–1.96 (m, 2H), 1.95–1.82 (m, 4H). ¹³C NMR (101 MHz, CDCl₃) δ 177.09, 166.52, 166.10, 163.68, 163.60, 163.40, 163.33, 143.73, 140.88, 140.53, 139.23, 138.58, 136.40, 134.77, 132.58, 131.87, 131.65, 131.04, 130.74, 130.10, 130.04, 129.14, 128.96, 128.82, 128.76, 127.99, 127.74, 127.41, 127.32, 126.96, 125.99, 125.51, 122.97, 122.59, 121.51, 121.10, 120.39, 116.63, 116.49, 56.27, 55.97, 55.89, 41.93, 41.41, 40.26, 39.86, 38.91, 38.79, 25.58, 25.41, 25.00, 20.54. HRMS (ESI; m/z). Calcd for C₆₀H₅₅N₇O₇Cl₂, [M+2H]²⁺, 528.6843; found, 528.6847.

N-(3-((3-(6-bromo-1,3-dioxo-1H-benzo[de]isoquinolin-2(3H)-yl)propyl)(methyl)amino)propyl)-10-(4-((3-((3-(6-bromo-1,3-dioxo-1H-benzo[de]isoquinolin-2(3H)-yl)propyl)(methyl)amino)propyl)carbamoyl)phenyl)-7-methyl-9-oxo-9,10-dihydroacridine-2-carboxamide (N14). A yellow solid was obtained with a yield of 65%. ¹H NMR (400 MHz, CDCl₃) δ 8.74–8.59 (m, 3H), 8.40 (d, J = 8.1 Hz, 2H), 8.38–8.33 (m, 1H), 8.27 (d, J = 8.2 Hz, 1H), 8.18 (d, J = 7.5 Hz, 3H), 8.07 (d, J = 7.8 Hz, 1H), 7.95 (dd, J = 9.0, 2.0 Hz, 1H), 7.83 (d, J = 7.5 Hz, 1H), 7.76 (d, J = 7.8 Hz, 1H), 7.62 (dd, J = 14.8, 7.1 Hz, 3H), 7.35 (d, J = 6.1 Hz, 2H), 7.08 (d, J = 8.6 Hz, 1H), 6.66 (d, J = 9.0 Hz, 1H), 6.42 (d, J = 7.8 Hz, 1H), 4.22–4.02 (m, 4H), 3.88–3.48 (m, 4H), 2.67 (d, J = 7.6 Hz, 8H), 2.43 (d, J = 10.2 Hz, 6H), 2.22 (s, 3H), 2.11–2.04 (m, 2H), 2.01 (s, 2H), 1.91 (s, 4H). ¹³C NMR (101 MHz, CDCl₃) δ 177.11, 166.59, 166.13, 163.58, 163.54, 163.50, 163.46, 143.76, 140.88, 140.52, 136.37, 134.83, 133.48, 133.45, 132.78, 132.59, 131.93, 131.69, 131.64, 131.14, 131.06, 130.85, 130.67, 130.54, 130.46, 130.25, 130.10, 130.06, 129.89, 128.73, 128.68, 127.99, 127.64, 125.98, 125.56, 122.96, 122.60, 122.11, 121.73, 121.21, 120.38, 116.65, 116.51, 56.19, 55.92, 55.85, 41.90, 41.37, 38.93, 38.79, 25.54, 25.37, 24.96, 20.61. HRMS (ESI; m/z). Calcd for C₅₉H₅₃Br₂N₇O₇, [M+2H]²⁺, 572.6338; found, 572.6328.

2.1.3. General procedure for the preparation of WZZO2

To a solution of N14 (0.16 mmol) and 1-methylpiperazine (0.48 mmol) in anhydrous N,N-dimethylformamide (10 mL) was added Pd/C (5% mol), NaO-*t*-Bu (0.224 mmol) and then dicyclohexyl-(2-phenylphenyl)phosphane (1% mol). The reaction mixture was stirred at 80 °C under nitrogen atmosphere for 10 h. The reaction mixture was quenched with 10 mL ice water, filtered, and the filtrate was extracted with dichloromethane (3 × 10 mL). The combined organic layer was washed with brine, dried over anhydrous sodium sulfate, filtered, and then concentrated under reduced pressure to give crude yellow solid WZZO2. The residue was purified by using chromatograph on silica gel with DCM/MeOH (30/1) to give the desire product.

7-methyl-N-(3-(methyl(3-(6-(4-methylpiperazin-1-yl)-1,3-dioxo-1H-benzo[de]isoquinolin-2(3H)-yl)propyl)amino)propyl)-10-(4-((3-(methyl(3-(6-(4-methylpiperazin-1-yl)-1,3-dioxo-1H-benzo[de]isoquinolin-2(3H)-yl)propyl)amino)propyl)carbamoyl)phenyl)-9-oxo-9,10-dihydroacridine-2-carboxamide (WZZO2). A yellow solid was obtained with a yield of 52%. ¹H NMR (400 MHz, CDCl₃) δ 8.82 (d, J = 1.6 Hz, 1H), 8.73 (s, 1H), 8.59 (s, 1H), 8.37–8.32 (m, 2H), 8.26 (d, J = 8.0 Hz, 4H), 8.17 (d, J = 8.2 Hz, 2H), 8.02–7.93 (m, 2H), 7.50 (dt, J = 22.6, 7.9 Hz, 2H), 7.32 (d, J = 8.2 Hz, 2H), 7.12 (d, J = 8.8 Hz, 1H), 7.02 (d, J = 8.1 Hz, 1H), 6.96 (d, J = 8.1 Hz, 1H), 6.71 (d, J = 9.0 Hz, 1H), 6.48 (d, J = 8.7 Hz, 1H), 4.21–4.15 (m, 2H), 4.10 (dd, J = 7.4, 3.6 Hz, 2H), 3.68 (d, J = 5.0 Hz, 2H), 3.62 (d, J = 5.6 Hz, 2H), 3.18 (s, 8H), 2.69 (s, 8H), 2.59 (dd, J = 12.1, 5.8 Hz, 8H), 2.40 (t, J = 7.1 Hz, 9H), 2.33 (s, 3H), 2.28 (s, 3H), 1.96 (dd, J = 15.1, 7.0 Hz, 4H), 1.90–1.80 (m, 4H). ¹³C NMR (101 MHz, CDCl₃) δ 177.41, 166.51, 166.21, 164.45, 164.35, 163.96, 163.85, 156.16, 155.69, 143.93, 140.86, 140.76, 136.46, 134.80, 132.56, 132.48, 132.40, 131.68, 131.01, 130.91, 130.61, 130.10, 129.69, 128.04, 126.36, 125.95, 125.93, 125.77, 125.50, 125.42, 123.10, 122.78, 121.56, 120.63, 116.76, 116.63, 116.54, 115.98, 114.78, 114.73, 56.69, 56.26, 56.13, 55.89, 55.11, 55.05, 52.88, 52.83, 46.11, 46.09, 41.98, 41.75, 40.21, 39.99, 38.63, 38.60, 31.93, 29.71, 25.91, 25.53, 25.20, 20.65. Purity was determined to be 96.03% by using HPLC. HRMS (ESI; m/z). Calcd for C₇₀H₇₇N₁₁O₇, [M+3H]³⁺, 395.5409; found, 395.5410.

2.2. DNA oligonucleotides

DNA oligonucleotides were purchased from Sangon (China) and dissolved in double distilled deionized water. Their concentrations were calculated based on the Beer–Lambert law ($A = \epsilon lc$) from the absorbance at 260 nm using a Nano Drop 1000 Spectrophotometer (Thermo Fisher Scientific, USA). All oligonucleotides were single-stranded as shown in Table S1, which were diluted with relevant buffers to working concentrations.

2.3. Surface plasmon resonance (SPR) experiment

SPR experiment was performed on a ProteOn XPR36 Protein Interaction Array system (Bio-Rad Laboratories, Hercules, CA) with a Neutravidin-coated GLH sensor chip. For immobilization, all DNA samples were biotinylated and attached to a streptavidin-coated sensor chip. Oligomer Py41 (5'-biotin-d[GCGTCCACCTCCCTGCCCCGCGCCCCCTTCTCCAGC]-3') was diluted to 400 nM with running buffer 20 mM 2-(4-morpholino)ethanesulfonic acid, pH 5.5, 100 mM KCl, 0.05% Tween-20. Oligomer Pu41 (5'-biotin-d[GCTGGGAGAAGGGGGGCGGGGCGAGGGGTGGACGC]-3') and duplex DNA (5'-biotin-d[TATAGCTATA-HEG-TATAGCTATA]-3') were diluted to 400 nM with running buffer 50 mM Tris-HCl, pH 7.4, 100 mM KCl. The DNA samples were then captured (1000 RU) in flow cells, and a blank cell was used as a control. Ligand solutions (at 0, 0.625, 1.25, 2.5, 5, 10 μM) were prepared with the running buffer by serial dilutions from stock solutions (10 μM in DMSO). Samples of six concentrations were injected at a flow rate of 25 mL/min for 200 s of association phase, followed with 300 s of dissociation phase at 25 °C. Between consecutive measurements, the GLH sensor chip was regenerated with short injection of 50 mM

NaOH. The final graphs were obtained by subtracting blank sensorgrams from the i-motif, G-quadruplex or duplex sensorgrams. Langmuir model was used for fitting kinetic data, which was analyzed with ProteOn manager software.

2.4. Microscale thermophoresis (MST) experiment

The 5'-end FAM labeled Py41, Pu41 and Duplex DNA were purchased from Sangon (China). By using the NT.115 MST instrument (NanoTemper, Germany), the thermophoresis movements of the fluorescently labeled nucleic acids and compound complexes were detected by monitoring the fluorescence distributions inside the capillary. The concentration of DNA was held constant at 1 μ M, and the compound was diluted at 3:4 from 10 μ M for 12 times. The samples were loaded into standard-treated MST-grade glass capillaries. The intensities of the LED and laser were set as 20% and 20%, respectively. Data were analyzed using NT Analysis 1.4.23 software.

2.5. CD and CD-melting experiments

The oligomers Py41 and Pu41 at final concentration of 2 μ M were diluted from stock with BPES buffer (pH 5.5). The samples were heated to 95 °C for 5 min, then gradually cooled to room temperature, and stored at 4 °C overnight. The CD spectra were recorded on a Chirascan (Applied Photo-physics, UK) spectrophotometer at 25 °C. A quartz cuvette with 1 mm path length was used for the spectra recorded over a wavelength range of 230–330 nm at 1 nm bandwidth, 1 nm step size, and 0.5 s per point. A buffer blank was subtracted for all spectra, and the spectra were averaged, smoothed, and baseline corrected to remove signal contribution from buffer. Final analysis of the data was carried out using graphpad 6.0. For CD melting experiments, samples were annealed at first, with i-motif and G-quadruplex formation induced. The molar ellipticity at 288 nm or 263 nm was measured over a temperature range of 25–95 °C, with the data calculated through graphpad 6.0.

2.6. Fluorescence resonance energy transfer (FRET) experiment

The oligonucleotides dual labeled fluorescently at 10 μ M concentration were used as FRET probes. FPY41T (5'-FAM-GCGTCCACCCTCCCTGCCCGCCGCCCCCTTCTCCAGC-TAMRA-3') was dissolved in 30 mM BPES buffer containing 1 mM EDTA and 100 mM KCl at pH 5.5. FPU41T (5'-FAM-GCTGGGA-GAAGGGGGGGCGGGCGGGCAGGGAGGGTGGACGC-TAMRA-3'), and F10T (5'-FAM-dTATAGCTATA-HEG-TATAGCTATA-TAMRA-3') with HEG linker of (-CH₂-CH₂-O)₆, were prepared as 10 μ M solution in 10 mM Tris-HCl buffer containing 10 mM KCl at pH 7.4. FAM is 6-carboxy-fluorescein as donor fluorophore, and TAMRA is 6-carboxytetramethylrhodamine as acceptor fluorophore. These oligonucleotides were thermally annealed. For the concentration-dependent FRET assays, an equal volume of the compound was added to probes, and the fluorescence intensity from 500 to 700 nm was measured by using LS-55 luminescence spectrophotometer (Perkin-Elmer, USA). The data were corrected with the signal of compound in the same buffer to obtain relative fluorescence intensity. Final analysis of data was performed using graphpad 6.0.

2.7. NMR experiment

The DNA oligonucleotides were purchased from Sangon (China). The final NMR samples were prepared in 10%/90% D₂O/H₂O solution at pH 5.5 or 6.8. The stock solution of compound was dissolved in d₆-DMSO, and concentration of DNA sample was 1.0 mM. ¹H NMR titration experiments were performed on Bruker DRX-600 MHz spectrometer at temperatures of 5 °C or 25 °C, with water signal suppressed in the experiment.

2.8. Cell culture

Human breast adenocarcinoma cell line MCF-7, human colon cancer cell line HCT116, human liver hepatocellular carcinoma cell line HepG2, human malignant melanoma cell line A375, human hepatocellular carcinoma cell line Huh7, and human embryonic kidney cell line HEK293, were all purchased from China Center for Type Culture Collection in Wuhan. The cell lines were cultivated in RPMI-1640 or DMEM medium configured with 10% fetal calf serum, 100 U/mL penicillin, and 100 mg/mL Streptomycin at 37 °C in a humidified atmosphere with 5% CO₂.

2.9. MTT cytotoxicity assay

Human breast adenocarcinoma cell line MCF-7, human colon cancer cell line HCT116, human liver hepatocellular carcinoma cell line HepG2, human malignant melanoma cell line A375, human hepatocellular carcinoma cell line Huh7, and human embryonic kidney cell line HEK293, were seeded on 96-well plates (5.0 × 10³ per well) with 100 μ L of culture medium, and incubated for 12 h at 37 °C in a humidified atmosphere with 5% CO₂, and then exposed to various concentrations of compounds. After 48 h of treatment at 37 °C in a humidified atmosphere of 5% CO₂, 20 μ L of 2.5 mg/mL methyl thiazolyl tetrazolium (MTT) solution was added to each well, and the mixture was further incubated for 4 h. The cells in each well were then treated with dimethyl sulfoxide (DMSO) (200 μ L for each well) and the culture medium was siphoned off, and the absorbance was recorded at 570 nm. All drug doses were parallel tested in triplicate, and the cytotoxicity was evaluated based on the percentage of cell survival in a dose-dependent manner regarding to the negative control. The final IC₅₀ values were determined by using the Graph Pad Prism 6.0.

2.10. Dual-Luciferase reporter assay

In this assay, 200 ng of constructed psiCHECK2 luciferase plasmid (Promega, USA) containing PDGFR- β wild type promoter was transfected into MCF-7 cells by using Lipofectamine 2000 (Invitrogen, USA). After 4 h, compounds were added to the cells at different concentration. The cells were incubated for 48 h at 37 °C in a humidified atmosphere with 5% CO₂, and the transfected cells were washed with ice-cold PBS to reduce the background signals from the medium. Luciferase assays were subsequently performed according to the manufacturer's instructions using the dual-luciferase assay system (Promega, USA). After a 1500 ms delay, secreted luciferase signals were collected for 10 s using a microplate reader (Molecular Devices, Flex Station 3, USA). The quantification was performed using a multimode reader (Molecular Devices). The secreted Renilla luciferase activity was normalized to the firefly luciferase activity.

2.11. RNA extraction and real time polymerase chain reaction (RT-PCR)

MCF-7 breast cancer cells were plated in 6-well plate (2 × 10⁵ cells/well), and incubated for 12 h at 37 °C in a humidified atmosphere with 5% CO₂. Then WZZ02 was added at final concentrations of 20, 10, 5, 2.5, 1.25 μ M or with DMSO as control. After incubation for 12 h, cells were harvested, and the RNA was extracted according to the manufacturer's instructions. Total RNA was used as a template for reverse transcription using the following protocol: For the first step, each 10 μ L reaction mixture containing 2.0 μ L 5 × gDNA Eraser buffer, 1.0 μ L gDNA Eraser, 1 μ g of total RNA, was incubated at 42 °C for 2 min, and then immediately cooled to 4 °C. For the second step, 1.0 μ L PrimeScript RT Enzyme Mix I, 4.0 μ L RT Primer Mix, 4.0 μ L 5 × PrimeScript Buffer 2 (for Real Time), RNase Free dH₂O 1.0 μ L, and the first step mixture 10 μ L, total to 20 μ L, were incubated at 37 °C for 15 min, then at 85 °C for 5 sec, last immediately cooled to 4 °C to obtain the cDNA, which was applied directly for further qPCR. The real-time PCR was performed on a real-time PCR apparatus (Roche LightCycler 480) according to the

manufacturer's protocol. The total volume of 20 μL of quantitative reaction mixtures contained 10 μL of SYBR Premix Ex Taq II (Tli RNaseH Plus, 2 \times , Takara, Japan), 0.8 μL PCR Forward Primer (10 μM), 0.8 μL PCR Reverse Primer (10 μM), and 2 μL of cDNA. The PDGFR- β mRNA levels were normalized to β -actin mRNA level of each sample. Results of real-time PCR were analyzed using the 2- ΔCT method.

2.12. Western blot

MCF-7 cells were seeded on 6-well plate (2×10^5 cells/well) and incubated for 12 h at 37 $^\circ\text{C}$ in a humidified atmosphere with 5% CO_2 . After incubation with **WZZ02** at final concentration of 10, 5, 2.5, 1.25, 0.625 μM or with the same volume of DMSO as control for 24 h, cells were harvested from each well of culture plates, and lysed in 100 μL of protein extraction buffer for 10 min. The suspension was centrifuged at 10,000 rpm at 4 $^\circ\text{C}$ for 15 min, and the protein content of supernatant was measured by using BCA assay. The same amount of protein for each sample was loaded onto 10% polyacrylamide gel at 100 V for 1.5 h, and then transferred to a microporous polyvinylidene difluoride (PVDF) membrane. Western blotting was performed by using anti-PDGFR- β and anti- β -actin (cell signaling technology) antibodies, as well as horseradish peroxidase-conjugated anti-rabbit secondary antibody. Protein bands were visualized by using chemiluminescence substrate.

2.13. FITC Annexin V/PI cell apoptosis detection

MCF-7 cells were seeded on 6-well plate (2×10^5 cells/well) and incubated for 12 h at 37 $^\circ\text{C}$ in a humidified atmosphere with 5% CO_2 . After incubation with **WZZ02** at final concentrations of 10, 5, 2.5, 1.25, 0.625 μM or with the same volume of DMSO as control for 24 h, the MCF-7 cells were digested by trypsin without EDTA. The suspension was centrifuged at 2000 rpm for 10 min, and the MCF-7 cells were then washed in PBS. FITC Annexin V/PI cell apoptosis detection was performed using the FITC Annexin V/PI Apoptosis Kit (Multi Sciences). The MCF-7 cells were resuspended in 500 μL binding buffer. FITC Annexin V (5 μL) and PI (10 μL) were added, and the cells were disturbed by gently vortexing the samples prior to incubation at room temperature (25 $^\circ\text{C}$) for 15 min in the dark. Emitted fluorescence was quantitated by using Epics Elite flow cytometry (Beckman Coulter, USA). For each analysis, 10,000 events were collected.

2.14. Cell cycle analysis

Cell cycle analysis for arrest detection was performed using the Cell Cycle Staining Kit (Multi Sciences). MCF-7 cells were seeded on 6-well plate (2×10^5 cells/well) and incubated for 12 h at 37 $^\circ\text{C}$ in a humidified atmosphere with 5% CO_2 . After incubation with **WZZ02** at final concentrations of 10, 5, 2.5, 1.25, 0.625 μM or with the same volume of DMSO as control for 24 h, MCF-7 cells were treated with trypsin, washed with PBS, fixed with 75% ethanol at -20 $^\circ\text{C}$ overnight, and then centrifuged and resuspended in a staining solution (50 $\mu\text{g}/\text{mL}$ PI, 75 KU/mL RNase A in PBS) for 30 min at room temperature in dark. The cells were analyzed by using flow cytometry with an Epics Elite XL flow cytometer (Beckman Coulter). For each analysis, 10,000 events were collected. The cell cycle distribution was analyzed with EXPO32 ADC software.

2.15. xCELLigence real time cellular analysis (RTCA)

MCF-7 cells were seeded on E-Plate 16 PET and cultured for about 16 h before treatment with increasing concentration of **WZZ02** or DMSO as a control. The cells were sampled every minute for 15 min. The data were obtained by using Graph Pad Prism 6.0.

2.16. Colony formation assays

MCF-7 cells were seeded on 6-well plate (1,000 cells/well) and incubated for 24 h at 37 $^\circ\text{C}$ in a humidified atmosphere with 5% CO_2 , and then exposed to **WZZ02** at final concentrations of 2.5, 1.25, 0.625, 0.3125 μM and DMSO as a control for 7 days. At last, the cells were fixed with methyl alcohol and dyed with crystal violet. The pictures were taken by using cell imager.

2.17. Cell scrape assay

MCF-7 cells were seeded on 6-well plate (300,000 cells/well) and incubated for 24 h at 37 $^\circ\text{C}$ in a humidified atmosphere with 5% CO_2 . A cross-shaped scrape was made through the monolayer MCF-7 cells using a plastic pipet tip, and then the cells were exposed to **WZZ02** at final concentrations of 5, 2.5, 1.25, 0.625, 0.3125 μM and DMSO as a control, respectively. Several wounded areas were observed and photographed using microscopy after scratching and then culturing for 0, 24 and 48 h. The edge of the cells was marked with a white line to observe obviously.

2.18. Evaluation of in vivo antitumor activity

BALB/c female nude mice (three weeks old) were purchased from and housed at the Experimental Animal Center of Sun Yat-sen University (Guangzhou, China) and maintained in pathogen-free conditions (12 h light-dark cycle at 24 ± 1 $^\circ\text{C}$ with 60–70% humidity and provided with food and water ad libitum). All procedures were approved by the Animal Care and Use Committee of Sun Yat-sen University and conformed to the legal mandates and national guidelines for the care and maintenance of laboratory animals. MCF-7 cells were harvested, pelleted through centrifugation at 800 rpm for 5 min, and resuspended in sterile serum-free medium without EDTA. The cells (1×10^6 in 100 μL) were then subcutaneously implanted into the underarm regions of 35 mice. Tumor sizes were determined through Vernier caliper measurements, and tumor volumes were calculated according to the formula: (shortest diameter)² \times (longest diameter)/2. When the tumor size reached approximately 100 mm^3 , the mice were randomly divided into five groups (seven mice per group) for intraperitoneal injection (ip) daily with either: the vehicle control group, 10 mg/kg **WZZ02** treated group, 5.0 mg/kg **WZZ02** treated group, 2.5 mg/kg **WZZ02** treated group, and Cisplatin 2.0 mg/kg treated group (five weeks). The tumor size and body weight of mice were measured once every 2 days after treatment, and growth curves were plotted using average tumor volume within each experimental group. At the end of the observation period, the animals were euthanized by cervical dislocation, and the tumors and organs were removed and weighed. The inhibition rate (IR) was calculated according to the formula: $\text{IR} = (1 - \text{Mean tumor weight of the experimental group} / \text{Mean tumor weight of the control group}) \times 100\%$.

3. Results

3.1. Chemistry

In an early study, we have synthesized and studied an acridone derivative **B19**, which can selectively bind to and stabilize oncogene *c-myc* promoter i-motif, resulting in down-regulation of *c-myc* transcription and translation, however its effect on tumor cells apoptosis requires improvement.⁴⁰ Therefore, we synthesized a variety of **B19** derivatives containing a known anti-cancer fluorescent chromophore naphthalimide for the purpose of enhancing anti-cancer activity. The synthetic pathway for acridone-naphthalimide derivatives was shown in [Scheme 1](#). 2-Amino-5-methylbenzoic acid (1) and 4-iodobenzoic acid (2) were used as starting materials for three step reactions to give key intermediate **5** through Ullmann reaction, intra-Friedel-Crafts acylation, and hydrolysis reaction. Next, 4-substituted-1,8-naphthalic anhydride (**6**) was reacted with various types of amines (7) to produce compound **8**

(L1-L14), which was then reacted with intermediate **5** to give compound **9** (N1-N14). After initial screening through SPR experiment, compound **N14** was found to have an optimal chain linker for selective binding with PDGFR- β gene promoter i-motif and G-quadruplex. It has been reported that *N*-methylpiperazine group can interact with G-quadruplex with high affinity in cells,⁴⁵ which was therefore incorporated into compound **N14** to produce compound **WZZ02** for improved binding affinity, through reaction with 1-methylpiperazine catalyzed with Pd/C and dicyclohexyl-(2-phenylphenyl)phosphane.

3.2. Interactive studies of acridone-naphthalimide derivative **WZZ02** with PDGFR- β gene promoter i-motif and G-quadruplex

SPR experiment was performed to evaluate binding affinity of **WZZ02** with various oncogene promoter i-motif and G-quadruplex, and we found that **WZZ02** could selectively bind with PDGFR- β gene promoter i-motif and G-quadruplex (Table S2), with their K_D values determined to be 3.12 and 3.23 μM respectively (Fig. S1A&B). MST experiment was also performed to verify the result, with the binding affinity of **WZZ02** to PDGFR- β promoter i-motif, G-quadruplex and duplex DNA determined to be $4.52 \pm 0.49 \mu\text{M}$, $6.11 \pm 0.48 \mu\text{M}$, and $529 \pm 74 \mu\text{M}$ (Fig. S2A-C). This indicated that **WZZ02** had good binding affinity with PDGFR- β promoter i-motif and G-quadruplex, without significant interaction to duplex DNA. For comparison, a well-known G-quadruplex binding ligand **TMPyP4** was used as a control, with its binding affinity to PDGFR- β promoter i-motif, G-quadruplex and duplex DNA determined to be $463 \pm 62 \mu\text{M}$, $3.96 \pm 0.35 \mu\text{M}$, and $1,310 \pm 78 \mu\text{M}$ through MST experiment (Fig. S2D-F). This indicated that **TMPyP4** had good binding affinity with PDGFR- β promoter G-quadruplex without significant interaction to PDGFR- β promoter i-motif and duplex DNA.

In order to know whether **WZZ02** could affect stability of PDGFR- β

promoter i-motif and G-quadruplex, we performed CD-melting experiment. Oligomer Py41 (2 μM) in BPES buffer at pH 5.5 with sequence of PDGFR- β promoter i-motif had melting temperature of 58.24 $^{\circ}\text{C}$ (Fig. S3), and addition of 10 μM **WZZ02** could reduce its melting temperature to 41.51 $^{\circ}\text{C}$, with ΔT_m value of $-16.73 \text{ }^{\circ}\text{C}$ (Fig. 2A). On the other hand, oligomer Pu41 (2 μM) in Tris-HCl buffer at pH 7.4 with sequence of PDGFR- β promoter G-quadruplex had melting temperature of 77.41 $^{\circ}\text{C}$ (Fig. S3), and addition of 10 μM **WZZ02** could increase its melting temperature to over 100 $^{\circ}\text{C}$, with ΔT_m value of $> 20 \text{ }^{\circ}\text{C}$ (Fig. 2B). Our results showed that **WZZ02** could both destabilize PDGFR- β promoter i-motif and stabilize PDGFR- β promoter G-quadruplex significantly. A well-known G-quadruplex binding ligand **TMPyP4** was used as a control for comparative studies. For oligomer Py41 (2 μM) in BPES buffer at pH 5.5, addition of 10 μM **TMPyP4** slightly increased its melting temperature to 58.35 $^{\circ}\text{C}$, with ΔT_m value of 0.11 $^{\circ}\text{C}$ (Fig. 2C). For oligomer Pu41 (2 μM) in Tris-HCl buffer at pH 7.4, addition of 10 μM **TMPyP4** significantly increased its melting temperature to over 100 $^{\circ}\text{C}$, with ΔT_m value of $> 20 \text{ }^{\circ}\text{C}$ (Fig. 2D). These results showed that **TMPyP4** could stabilize PDGFR- β promoter G-quadruplex without significant effect on PDGFR- β promoter i-motif.

In order to confirm binding interactions of **WZZ02** to PDGFR- β gene promoter i-motif and G-quadruplex, we performed CD experiment. Oligomer Py41 showed a positive peak at 280–300 nm and a negative peak near 260 nm under acidic conditions (Fig. S3), which indicated the formation of i-motif structure.^{37,38} Upon addition of increasing concentration of **WZZ02**, the positive peak at 280–300 nm was decreased significantly in a dose-dependent manner (Fig. 3A), indicating strong interaction of **WZZ02** with PDGFR- β promoter i-motif. Oligomer Pu41 showed a positive peak at 265 nm and a negative peak near 240 nm in Tris-HCl buffer at pH 7.4, which indicated the formation of parallel G-quadruplex structure. Upon addition of increasing concentration of

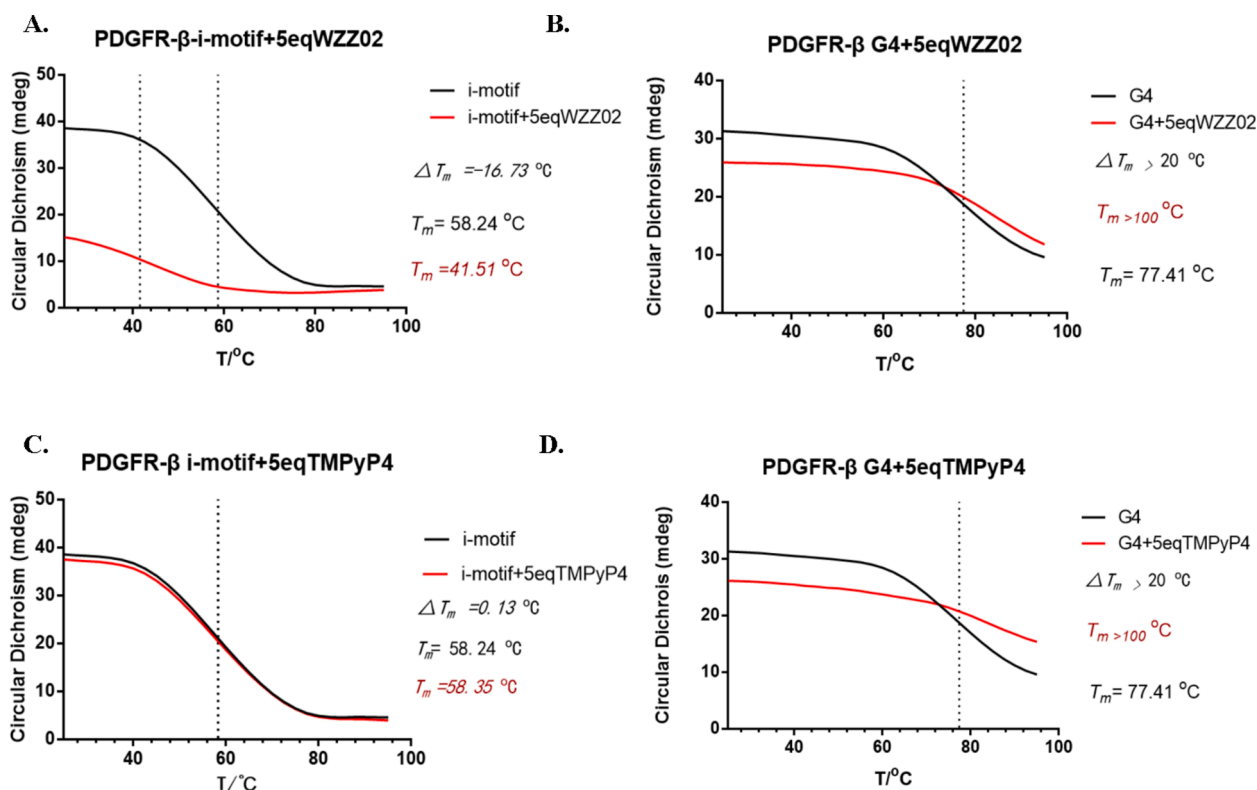


Fig. 2. CD-melting experiment for effect of **WZZ02** and **TMPyP4** on stability of oligomer Py41 with sequence of PDGFR- β gene promoter i-motif and oligomer Pu41 with sequence of PDGFR- β gene promoter G-quadruplex. (A) CD-melting experiment for effect of 10 μM **WZZ02** on stability of 2 μM oligomer Py41 in BPES buffer at pH 5.5, measured at 288 nm. (B) CD-melting experiment for effect of 10 μM **WZZ02** on stability of 2 μM oligomer Pu41 in Tris-HCl buffer at pH 7.4, measured at 263 nm. (C) CD-melting experiment for effect of 10 μM **TMPyP4** on stability of 2 μM oligomer Py41 in BPES buffer at pH 5.5, measured at 288 nm. (D) CD-melting experiment for effect of 10 μM **TMPyP4** on stability of 2 μM oligomer Pu41 in Tris-HCl buffer at pH 7.4, measured at 263 nm.

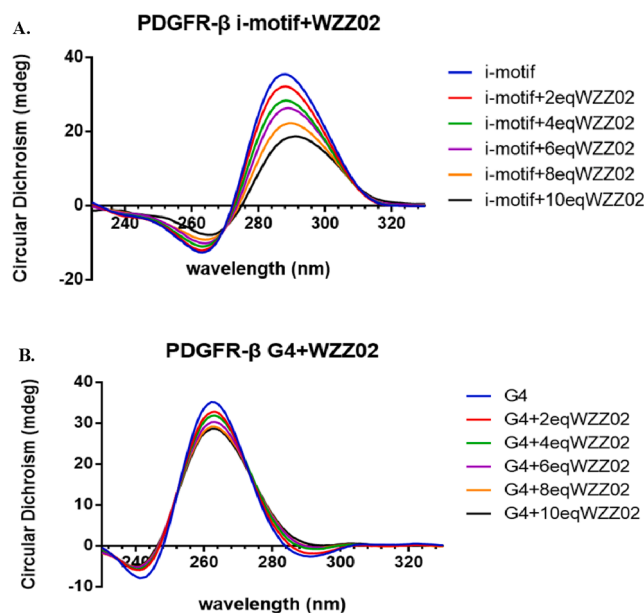


Fig. 3. CD experiments for effect of **WZZ02** on oligomer Py41 with sequence of PDGFR- β gene promoter i-motif and oligomer Pu41 with sequence of PDGFR- β gene promoter G-quadruplex. (A) CD experiment for addition of increasing concentration of **WZZ02** to oligomer Py41 in BPES buffer at pH 5.5. (B) CD experiment for addition of increasing concentration of **WZZ02** to oligomer Pu41 in Tris-HCl buffer at pH 7.4.

WZZ02, the positive peak at 265 nm was also decreased in a dose-dependent manner (Fig. 3B), indicating interaction of **WZZ02** with PDGFR- β promoter G-quadruplex.

Fluorescence resonance energy transfer (FRET) experiment was also performed to further analyze binding interactions of **WZZ02** to PDGFR- β gene promoter i-motif and G-quadruplex. Oligomer FPy41T with sequence of PDGFR- β promoter i-motif and oligomer FPu41T with sequence of PDGFR- β promoter G-quadruplex, were both dual labeled with FAM and TAMRA at 5' and 3'-end. Oligomer FPy41T showed pH-dependent spectral change, indicating its pH-dependent conformational change. I585/I518 ratio was determined to be 5.46 at pH 6.2, indicating formation of i-motif structure with two dyes at closer distance under relatively acidic condition. In comparison, I585/I518 ratio was determined to be 0.97 at pH 6.4, indicating unfolding of i-motif structure with two dyes at longer distance under relatively basic condition (Fig. 4A). Upon addition of increasing concentration of **WZZ02** to oligomer FPy41T, I585/I518 ratio was decreased in a dose-dependent manner, indicating its unfolding of i-motif structure (Fig. 4B). On the other hand, upon addition of increasing concentration of **WZZ02** to oligomer FPu41T, I585/I518 ratio was increased in a dose-dependent manner, indicating its stabilization of G-quadruplex structure. These results showed that **WZZ02** could unfold PDGFR- β promoter i-motif, and induce the formation of PDGFR- β promoter G-quadruplex, which are consistent with our CD-melting experimental results.

For comparison, FRET experiment was also performed to analyze effect of **TMPyP4** on conformational change of PDGFR- β gene promoter i-motif and G-quadruplex. As shown in Fig. S4A, I585/I518 ratio of oligomer FPy41T for PDGFR- β promoter i-motif was not affected upon addition of increasing concentration of **TMPyP4**. In contrast, I585/I518 ratio of oligomer FPu41T for PDGFR- β promoter G-quadruplex was increased in a dose-dependent manner upon addition of increasing concentration of **TMPyP4** (Fig. S4B). These results showed that **TMPyP4** could induce the formation of PDGFR- β promoter G-quadruplex without significant effect on PDGFR- β promoter i-motif, which are also consistent with our CD-melting experimental results.

The interaction of **WZZ02** with Py41 was further characterized by

using NMR experiments. The characteristics for the formation of hemi-protonated C—C⁺ base pairs in i-motif structure were imino proton peaks at 15–16 ppm, which indicated the formation of PDGFR- β promoter i-motif^{38,39} (Fig. S5). The i-motif structure was relatively stable under acidic condition at pH 5.5, which was unfolded under neutral condition at pH 6.8. At pH 5.5, upon addition of increasing concentration of **WZZ02** to Py41, the imino proton peaks at 15–16 ppm were decreased in a dose-dependent manner (Fig. S5A–C), indicating that **WZZ02** could unfold PDGFR- β promoter i-motif. This result is also consistent with above experimental data.

3.3. **WZZ02** down-regulated PDGFR- β gene transcription and translation in MCF-7 cells through interaction with its promoter G-quadruplex and i-motif

In order to investigate effect of **WZZ02** on PDGFR- β gene transcription and translation, several experiments were performed, including dual-luciferase reporter assay, reverse transcription-polymerase chain reaction (RT-PCR), and Western blot. Dual-luciferase reporter assay was performed with a pscheck2 plasmid carrying PDGFR- β gene promoter in front of the *Renilla Firefly* luciferase gene. After transfection, MCF-7 cells were incubated with **WZZ02** at increasing concentration for 48 h. **WZZ02** was found to significantly reduce the ratio of the *Renilla*/*Firefly* luciferase activity in a dose-dependent manner, as shown in Fig. S6.

Then, reverse transcription-polymerase chain reaction (RT-PCR) was performed to determine effect of **WZZ02** on regulation of PDGFR- β gene transcription in MCF-7 cells, through measurement of mRNA levels. As shown in Fig. 5A, **WZZ02** significantly down-regulated PDGFR- β gene transcription in a dose-dependent manner measured through qRT-PCR, upon incubation of MCF-7 cells with increasing concentration of **WZZ02** for 12 h. In comparison with **WZZ02**, **TMPyP4** showed relatively mild effect in down-regulating PDGFR- β gene transcription in a dose-dependent manner, as shown in Fig. 5B. Next, we studied effect of **WZZ02** on PDGFR- β gene expression, as shown in Fig. 5C. **WZZ02** significantly down-regulated PDGFR- β gene expression in a dose-dependent manner measured through Western blot, upon incubation of MCF-7 cells with increasing concentration of **WZZ02** for 24 h. As mentioned above, **WZZ02** could bind to both PDGFR- β gene promoter G-quadruplex and i-motif. **TMPyP4** could bind to PDGFR- β gene promoter G-quadruplex only without significant effect on i-motif, which was used for comparison. Our above results showed that **WZZ02** could significantly down-regulate PDGFR- β gene transcription and translation in MCF-7 cells possibly through its binding to PDGFR- β gene promoter G-quadruplex and i-motif. Our present result indicated that effect of **WZZ02** in destabilizing PDGFR- β promoter i-motif or their interactions could make further positive contribution in down-regulating PDGFR- β gene transcription.

3.4. Effect of **WZZ02** on MCF-7 cells proliferation, metastasis, apoptosis and cycle arrest

MTT assay was employed to evaluate the activity of **WZZ02** against human breast adenocarcinoma cell line MCF-7, human colon cancer cell line HCT116, human liver hepatocellular carcinoma cell line HepG2, human malignant melanoma cell line A375, and human hepatocellular carcinoma cell line Huh7. Treatment of MCF-7 cells with increasing concentration of **WZZ02** led to a remarkable arrest of cell growth in a dose-dependent manner with IC₅₀ value of 4.69 μ M, comparing with its effect on human normal liver cell HEK293 with IC₅₀ value of over 50 μ M (Table S3). To further evaluate the effect of **WZZ02**, RTCA assays were carried out for MCF-7 cells incubated with increasing concentration of **WZZ02** (0.625, 1.25, 2.5 μ M) for 90 h. RTCA plots were obtained using RTCA software 1.1.2, as shown in Fig. S7. The effect of **WZZ02** on growth arrest of MCF-7 cells was studied upon incubation of MCF-7 cells with increasing concentration of **WZZ02** for 48 h. **WZZ02** was found to have a significant effect with its IC₅₀ value determined to be 2.74 \pm

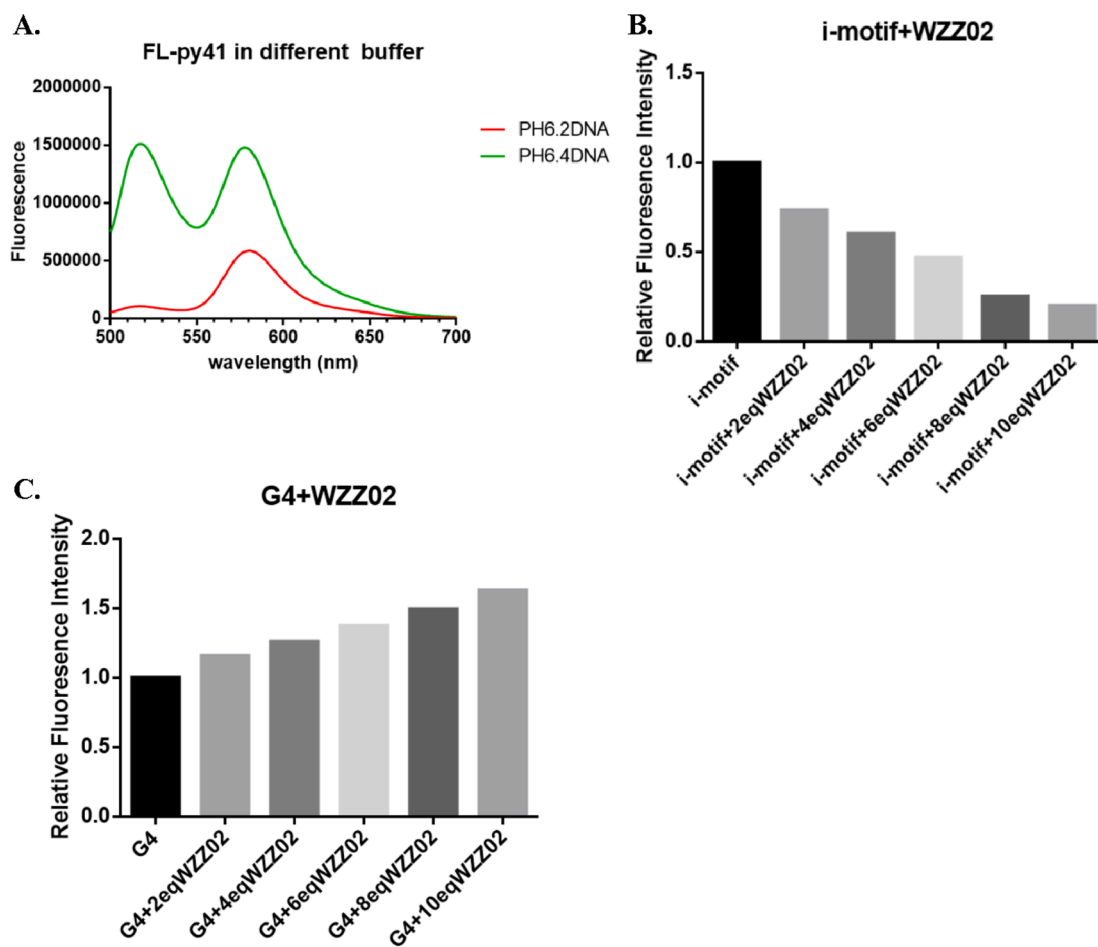


Fig. 4. FRET experiment for effect of **WZZ02** on oligomer FPpy41T with sequence of PDGFR- β gene promoter i-motif and oligomer FPy41T with sequence of PDGFR- β gene promoter G-quadruplex, which were both dual labeled with FAM and TAMRA at 5' and 3'-end. (A) Oligomer FPy41T showed pH-dependent spectral change, indicating its conformational change. I585/I518 ratio was determined to be 5.46 at pH 6.2, indicating formation of i-motif structure with two dyes at closer distance. In comparison, I585/I518 ratio was determined to be 0.97 at pH 6.4, indicating unfolding of i-motif structure with two dyes at longer distance. (B) FRET experiment for addition of increasing concentration of **WZZ02** to oligomer FPy41T in BPES buffer at pH 6.2. I585/I518 ratio was decreased in a dose-dependent manner, indicating its unfolding of i-motif structure. (C) FRET experiment for addition of increasing concentration of **WZZ02** to oligomer FPy41T in Tris-HCl buffer at pH 7.4. I585/I518 ratio was increased in a dose-dependent manner, indicating its stabilization of G-quadruplex structure.

0.43 μM (Fig. S7). Effect of **WZZ02** on migration or invasion of MCF-7 cells was also studied as shown in Fig. S8. **WZZ02** could suppress the migration of MCF-7 cells in both dose-dependent and time-dependent manners in cell scrape experiment.

Effect of **WZZ02** on apoptosis of MCF-7 cells was also studied as shown in Fig. 6. MCF-7 cells were incubated with increasing concentration of **WZZ02** (0, 1.25, 2.5, and 5 μM), followed with analysis for apoptosis using Annexin-FITC/PI double-staining flow cytometry. MCF-7 cell apoptosis was increased in a dose-dependent manner, upon incubation with increasing concentration of **WZZ02**. **WZZ02** could induce significant increase of MCF-7 cells in the early apoptosis from 0.28% to 33.5%, and remarkable increase of MCF-7 cells in the late apoptosis phase from 0.0% to 51.1%. Effect of **WZZ02** on long-term (7 days) proliferation of MCF-7 cells was also examined through colony formation experiment, as shown in Fig. 7. **WZZ02** could apparently inhibit proliferation of MCF-7 cells in a dose-dependent manner. Cell cycle analysis of MCF-7 cells was also performed with flow cytometry upon incubation with **WZZ02** for 48 h followed with propidium iodide (PI) staining. The percentage of cells was determined for each phase of the cell cycle. As shown in Fig. S9, after 48 h incubation with increasing concentration of **WZZ02**, MCF-7 cells in G2/M phase increased from 15.8% to 31.5%, and MCF-7 cells in G0/G1 phase decreased from 75.7% to 48.1%. The effect of **WZZ02** on cell cycle was found to be

concentration dependent, which suggested that **WZZ02** induced a cell cycle arrest in G2/M phase.

3.5. Effect of **WZZ02** on tumor growth in MCF-7 cervical xenograft

Since above results showed that **WZZ02** could down-regulate PDGFR- β gene transcription and inhibit tumor cells growth, its anti-tumor activity was further evaluated against a human cervical cancer xenograft (MCF-7) in athymic nude mice, as shown in Fig. 8. When the tumor size reached approximately 100 mm^3 , the mice were randomly divided into five groups (seven mice per group) for intraperitoneal injection (ip) once a day including: vehicle group, **WZZ02** 2.5 mg/kg treated group, **WZZ02** 5.0 mg/kg treated group, **WZZ02** 10 mg/kg treated group, and Cisplatin 2.0 mg/kg treated group. The tumors were collected after 34 days of treatment and analyzed. As shown in Fig. 8 and Fig. S10, compared with the vehicle group (mean of 1,511.1 mg), the treatment with compound **WZZ02** at 2.5 mg/kg, 5.0 mg/kg, and 10 mg/kg resulted in a statistically significant reduction of tumor weight in a dose-dependent manner, with a tumor growth inhibition ratio (IR) of 34.9%, 47.6%, and 56.5%, respectively (tumor weight mean values of 983.1 mg, 791.4 mg, and 657.8 mg). The wide-spectrum antitumor drug cisplatin was injected at dosage of 2 mg/kg as a positive control, to give a tumor growth inhibition ratio of 69.6%, with tumor weight mean

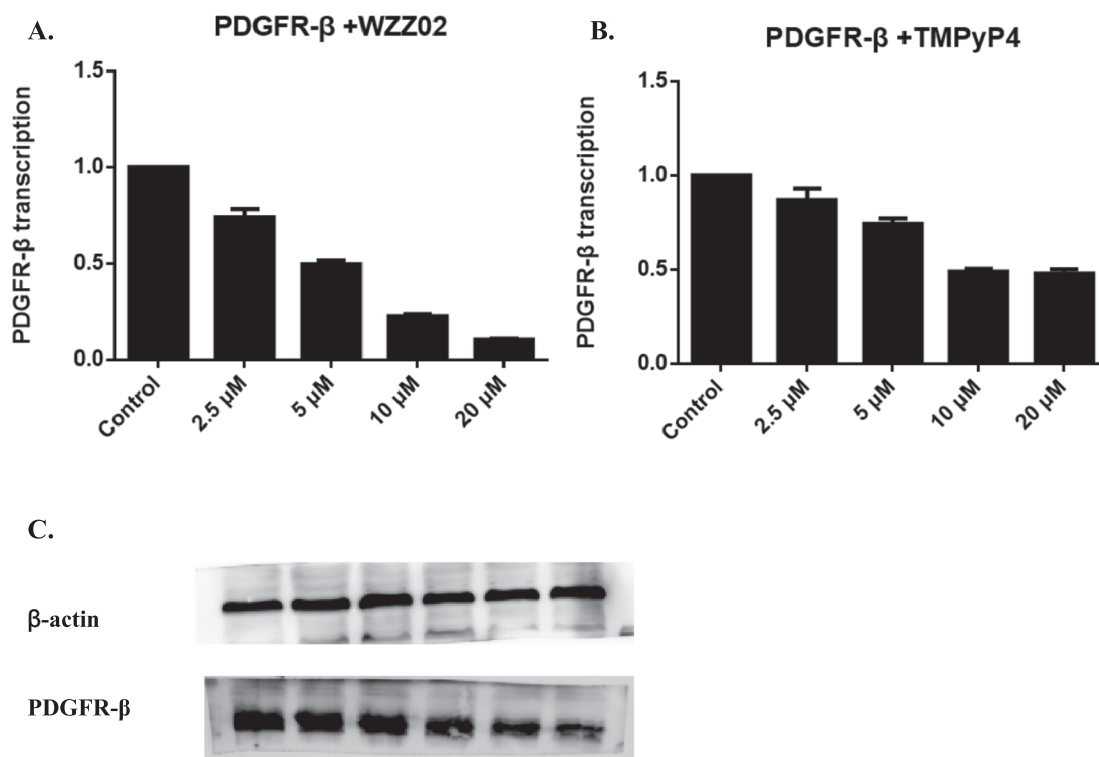


Fig. 5. Effect of **WZZ02** and **TMPyP4** on PDGFR- β gene transcription and translation in MCF-7 cells. (A) **WZZ02** down-regulated PDGFR- β gene transcription in a dose-dependent manner measured through qRT-PCR, upon incubation of MCF-7 cells with increasing concentration of **WZZ02** for 12 h, with β -actin used as an internal standard. (B) **TMPyP4** down-regulated PDGFR- β gene transcription in a dose-dependent manner measured through qRT-PCR, upon incubation of MCF-7 cells with increasing concentration of **TMPyP4** for 12 h, with β -actin used as an internal standard. (C) **WZZ02** down-regulated PDGFR- β gene expression in a dose-dependent manner measured through Western blot, upon incubation of MCF-7 cells with increasing concentration of **WZZ02** for 24 h, with β -actin used as an internal standard.

value of 458.7 mg (Fig. 8B). Meanwhile, the results of tumor volume from each group were consistent with results of tumor weigh. The treatment with **WZZ02** at dosage of 2.5 mg/kg, 5.0 mg/kg, and 10 mg/kg resulted in significant decrease of the final tumor volume in a dose-dependent manner (mean values of 985.1 mm³, 780.0 mm³, and 640.2 mm³ respectively), comparing with vehicle group (mean value of 1,530.0 mm³, Fig. 8A). As shown in Fig. 8C, no significant differences in body weights were observed among vehicle group and **WZZ02** treated groups. **WZZ02** neither altered cellular morphology nor induced pathological changes in the weight of mice and their heart, liver, spleen, and kidney (Fig. 8C&D), indicating that it was tolerated well at these doses. Although Cisplatin had a relatively strong effect on tumor, it also caused obviously systematic toxicity to organs. As shown in Fig. 8C&D, as the concentration of Cisplatin increase, the weight of mice and organs gradually declined, with apparent damage to the organs, as shown in Fig. S10B. Our above result showed that **WZZ02** exhibited a good antitumor activity with the inhibition of MCF-7 cancer cell growth in MCF-7 xenografts of BALB/C-nu/nu mice possibly through down-regulating PDGFR- β gene transcription.

4. Discussion

The PDGFR- β signaling pathway is a validated and important target for the treatment of certain malignant and nonmalignant tumors.^{46–49} It has been demonstrated that down-regulation of PDGFR- β expression can diminish the PDGFR- β -driven tumor effectively,⁵⁰ and therefore it is essential to develop new strategies targeting the PDGFR- β signaling pathway.⁴⁶ Our results provided an effective method for regulating PDGFR- β signaling pathway by small molecule interacting with both G-quadruplex and i-motif of PDGFR- β gene promoter. Previous studies have been mainly focused on G-quadruplex only, and our present data

indicated that G-quadruplex and i-motif in PDGFR- β gene promoter are both important in controlling PDGFR- β gene expression.

TMPyP4 is a well-known G-quadruplex binding ligand, which could stabilize PDGFR- β gene promoter G-quadruplex without significant effect on PDGFR- β gene promoter i-motif. Comparing with **TMPyP4**, **WZZ02** could similarly stabilize PDGFR- β gene promoter G-quadruplex but significantly destabilize PDGFR- β gene promoter i-motif. Since **WZZ02** showed more significant effect of downregulating PDGFR- β gene transcription, the destabilization of PDGFR- β gene promoter i-motif by **WZZ02** or their interactions could make strong positive contribution in downregulating PDGFR- β gene transcription. The destabilization of PDGFR- β gene promoter i-motif by **WZZ02** was strongly supported by our FRET assay and CD-melting experiment, which could be possibly due to binding interactions of **WZZ02** to the i-motif. These binding interactions or destabilization of the i-motif could prevent its binding with activating transcription factor resulting in downregulation of PDGFR- β gene expression. Since PDGFR- β mRNA could also contain G-quadruplex or i-motif on its 5'UTR, it is necessary to know whether **WZZ02** could affect stability of PDGFR- β mRNA. Actinomycin D is a known antibiotic inhibiting mRNA synthesis. Our incubation of MCF-7 cells with Actinomycin D in the presence and absence of **WZZ02** showed almost the same degradation velocity of PDGFR- β mRNA, indicating that **WZZ02** had no significant effect on stability of PDGFR- β mRNA, and its effect on translational level decrease is solely due to the decrease in transcription.

It has been previously reported that the stabilization of promoter i-motif by small molecule could upregulate BCL2 gene transcription.⁵¹ G-quadruplex and i-motif structures have been suggested to exist in a mutually exclusive fashion, and these two types of structures have been shown to mainly exist in different cell cycle stages.²⁶ It is likely that their mutual exclusivity in cells is regulated by relevant expression levels of DNA binding proteins related with cell signaling pathways. G-

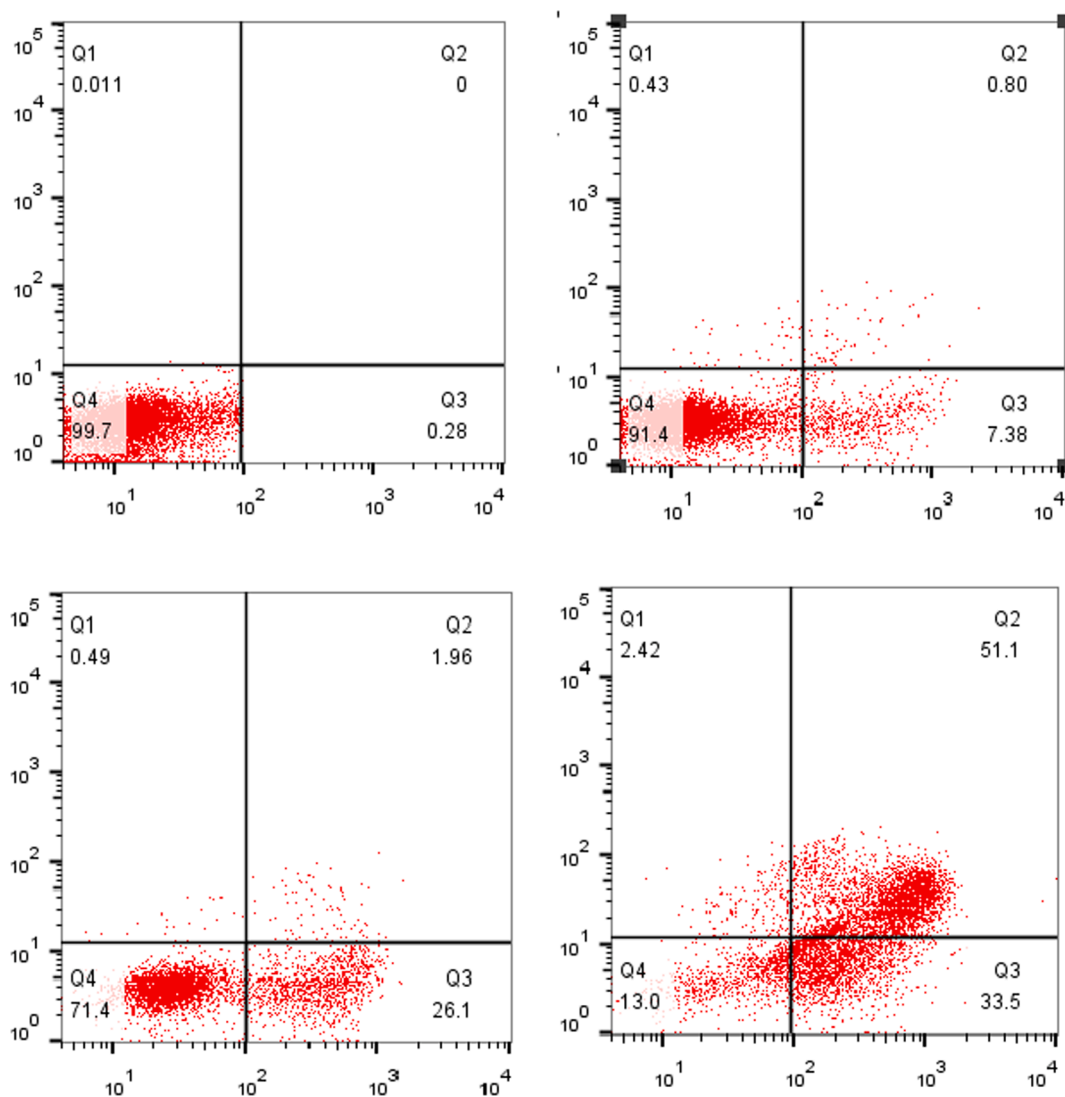


Fig. 6. MCF-7 cells were incubated with increasing concentration of WZZ02 (0, 1.25, 2.5, and 5.0 μM), followed with analysis for apoptosis using Annexin-FITC/PI double-staining flow cytometry.

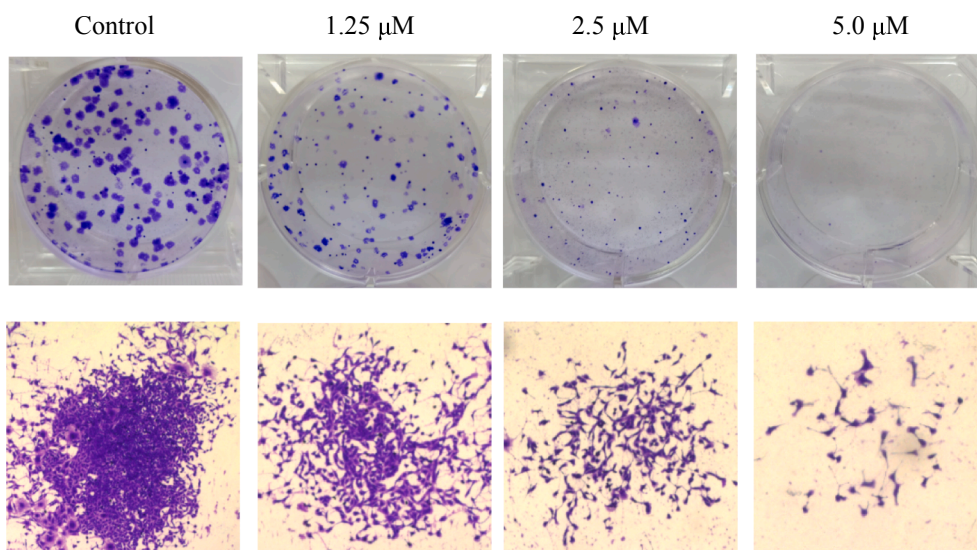


Fig. 7. Effect of WZZ02 on long-term (7 days) proliferation of MCF-7 cells.

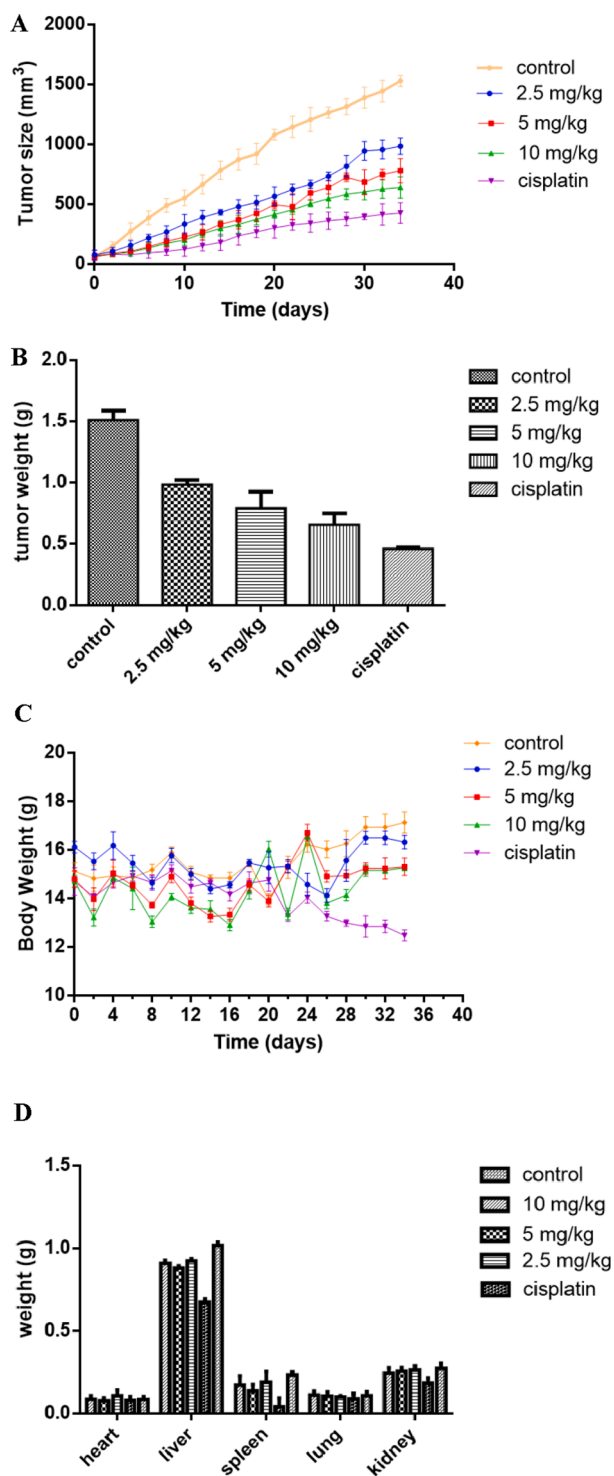


Fig. 8. Evaluation of the tumor growth inhibition by WZZ02 in MCF-7 xenograft model. WZZ02, Cisplatin, and saline (as vehicle) were administered through ip injection to athymic nude mice with human tumor xenografts established using MCF-7 cells. The mice were injected ip once a day for 34 days. Vehicle controls were injected with 100 μ L of saline. The positive control group received Cisplatin through ip injection at a dose of 2.0 mg/kg, once a day. Compound WZZ02 was similarly administered to mice, once a day, at doses of 2.5, 5.0 and 10 mg/kg, respectively. (A) The tumor sizes were measured and recorded every two days. The tumor volumes were calculated from sizes measured and recorded every day. The volume (mm^3) = length (mm) \times width (mm)²/2. (B) The tumor weight at the end of treatment. (C) The body weights were measured and recorded every two days. (D) Organ weights of the mice in each group at the end of observation period.

quadruplexes largely act as transcriptional repressors, while i-motifs could possibly act as either transcriptional activators or repressors. Our present results indicated that stabilization of promoter i-motif could upregulate PDGFR- β gene transcription, and therefore PDGFR- β gene promoter i-motif could possibly act as a transcriptional activator. For *in vitro* studies, WZZ02 showed stabilization of PDGFR- β gene promoter G-quadruplex but destabilization of PDGFR- β gene promoter i-motif at molecular levels, which are possibly due to their different binding modes and could be further studied in the future by a research group expert in structural determination.

Previously, we have synthesized and studied an acridone derivative B19, which can selectively bind to and stabilize oncogene *c-myc* promoter i-motif, however its effect on tumor cells apoptosis is not good enough.⁴⁰ Therefore, a known anti-cancer fluorescent chromophore naphthalimide was introduced to derivative B19 for the purpose of enhancing anti-cancer activity. It has been shown that naphthalimide chromophore can form stacking interactions with DNA adenine bases⁴¹ with strong anti-cancer activity.^{42–44} On the other hand, *N*-methylpiperazine group has been shown to interact with G-quadruplex with high affinity in cells,⁴⁵ which was also introduced to derivative B19 to give final product, acridone-naphthalimide derivative WZZ02. WZZ02 had strong binding affinity to PDGFR- β promoter i-motif and G-quadruplex with its K_D values determined to be 3.12 and 3.23 μ M through SPR experiment, which was also confirmed through MST experiment. WZZ02 could bind to both G-quadruplex and i-motif resulting in significant down-regulation of PDGFR- β gene transcription selectively, with potent anti-cancer activity. In comparison, neither acridone nor naphthalimide alone had significant binding to PDGFR- β gene promoter G-quadruplex and i-motif, with their K_D values determined to be all over 50 μ M. WZZ02 showed potent activity to various types of cancer cells including MCF-7, HCT116, HepG2, A375, and Huh7 cells with its IC_{50} values determined to be 4.69, 3.08, 9.62, 3.09, and 3.52 μ M. In comparison, neither acridone nor naphthalimide alone had significant effect on these types of cancer cells, with their IC_{50} values determined to be all over 20 μ M. Our results strongly indicated that WZZ02 targeted on both G-quadruplex and i-motif of PDGFR- β gene promoter in cells, resulting in down-regulation of PDGFR- β gene transcription selectively, leading to its potent anti-cancer activity.

It should be noted that WZZ02 could have a variety of other potential medical applications because of its naphthalimide fluorescent chromophore. It has been reported that the derivatives of 1,8-naphthalimide have various photophysical and biological properties and possibly function as free radical scavengers,⁵² fluorescent labels,⁵³ photoredox agents/photosensitizers,⁵⁴ and imaging agents.^{55–58} The derivatives of 1,8-naphthalimide are particularly attractive as fluorophores, because of their high quantum yields and photo-stability, with their fluorescence possibly tuned throughout a wide spectral range from blue to red.⁵⁹ It has also been shown that the derivatives of 1,8-naphthalimide could possibly function as fluorescent pigments and dyes,⁶⁰ fluorescent sensors for specific metal cations,^{61,62} pH sensors,⁶³ optical switches,⁶⁴ and organic luminescent devices.^{65–67} The wide properties for the derivatives of 1,8-naphthalimide could facilitate further in-depth mechanistic studies of WZZ02 through other fluorescent physical and chemical methods, which could help to further understand the function of PDGFR- β promoter G-quadruplex and i-motif. Our present results showed that WZZ02 could become a potential lead compound for further development for cancer treatment with improved potency and selectivity.

Declaration of Competing Interest

The authors declare that they have no known competing financial interests or personal relationships that could have appeared to influence the work reported in this paper.

Acknowledgements

We thank the National Natural Science Foundation of China (Grant 21977123), the Guangdong Basic and Applied Basic Research Foundation (Grant 2019A1515011074), the Natural Science Foundation of Guangdong Province (Grants 2017A030313089, 2017A030308003), and the Guangdong Provincial Key Laboratory of Construction Foundation (2017B030314030) for financial support of this study.

Appendix A. Supplementary material

Supplementary data to this article can be found online at <https://doi.org/10.1016/j.bmc.2021.116042>.

References

- 1 Farooqi AA, Siddik ZH. Platelet-derived growth factor (PDGF) signalling in cancer: rapidly emerging signalling landscape. *Cell Biochem Funct.* 2015;33:257–265. <https://doi.org/10.1002/cbf.3120>.
- 2 Wang KB, Dickerhoff J, Wu G, Yang D. PDGFR-beta Promoter Forms a Vacancy G-Quadruplex that Can Be Filled in by dGMP: Solution Structure and Molecular Recognition of Guanine Metabolites and Drugs. *J Am Chem Soc.* 2020;142:5204–5211. <https://doi.org/10.1021/jacs.9b12770>.
- 3 Demoulin JB, Essaghir A. PDGF receptor signaling networks in normal and cancer cells. *Cytokine Growth Factor Rev.* 2014;25:273–283. <https://doi.org/10.1016/j.cytogr.2014.03.003>.
- 4 Chen J, Yuan W, Wu L, Tang Q, Shu X. PDGF-D promotes cell growth, aggressiveness, angiogenesis and EMT transformation of colorectal cancer by activation of Notch1/Twist1 pathway. *Oncotarget.* 2017;8:9961–9973. <https://doi.org/10.18632/oncotarget.14283>.
- 5 Zhang N, Hu H, Fu Y, He F, Wang L. The overexpression of PDGF-BB and its receptor is correlated with lymphatic metastasis in patients with non-small cell lung cancer. *Int J Clin Exp Pathol.* 2018;11:6010–6017.
- 6 Heldin C. Targeting the PDGF signaling pathway in tumor treatment. *Cell Commun Signal.* 2013;11:97. <https://doi.org/10.1186/1478-811X-11-97>.
- 7 Onel B, Carver M, Agrawal P, Hurley LH, Yang D. The 3'-end region of the human PDGFR-beta core promoter nucleases hypersensitive element forms a mixture of two unique end-insertion G-quadruplexes. *Biochim Biophys Acta, Gen Subj.* 1862;2018:846–854. <https://doi.org/10.1016/j.bbagen.2017.12.011>.
- 8 Qin Y, Fortin JS, Tye D, Gleason-Guzman M, Brooks TA, Hurley LH. Molecular cloning of the human platelet-derived growth factor receptor beta (PDGFR-beta) promoter and drug targeting of the G-quadruplex-forming region to repress PDGFR-beta expression. *Biochemistry-US.* 2010;49:4208–4219. <https://doi.org/10.1021/bi100330w>.
- 9 Simonson T, Pecinka P, Kubista M. DNA tetraplex formation in the control region of c-myc. *Nucleic Acids Res.* 1998;26:1167–1172. <https://doi.org/10.1093/nar/26.5.1167>.
- 10 Siddiqui-Jain A, Grand CL, Bearrs DJ, Hurley LH. Direct evidence for a G-quadruplex in a promoter region and its targeting with a small molecule to repress c-MYC transcription. *Proc Natl Acad Sci USA.* 2002;99:11593–11598. <https://doi.org/10.1073/pnas.182256799>.
- 11 Sun D, Guo K, Rusche JJ, Hurley LH. Facilitation of a structural transition in the polypurine/polypyrimidine tract within the proximal promoter region of the human VEGF gene by the presence of potassium and G-quadruplex-interactive agents. *Nucleic Acids Res.* 2005;33:6070–6080. <https://doi.org/10.1093/nar/gki917>.
- 12 De Armond R, Wood S, Sun D, Hurley LH, Ebbinghaus SW. Evidence for the presence of a guanine quadruplex forming region within a polypurine tract of the hypoxia inducible factor 1alpha promoter. *Biochemistry-US.* 2005;44:16341–16350. <https://doi.org/10.1021/bi051618u>.
- 13 Dai J, Dexheimer TS, Chen D, et al. An intramolecular G-quadruplex structure with mixed parallel/antiparallel G-strands formed in the human BCL-2 promoter region in solution. *J Am Chem Soc.* 2006;128:1096–1098. <https://doi.org/10.1021/ja055636a>.
- 14 Dexheimer TS, Sun D, Hurley LH. Deconvoluting the structural and drug-recognition complexity of the G-quadruplex-forming region upstream of the bcl-2 P1 promoter. *J Am Chem Soc.* 2006;128:5404–5415. <https://doi.org/10.1021/ja0563861>.
- 15 Cogoi S, Xodo LE. G-quadruplex formation within the promoter of the KRAS proto-oncogene and its effect on transcription. *Nucleic Acids Res.* 2006;34:2536–2549. <https://doi.org/10.1093/nar/gkl286>.
- 16 Xu Y, Sugiyama H. Formation of the G-quadruplex and i-motif structures in retinoblastoma susceptibility genes (Rb). *Nucleic Acids Res.* 2006;34:949–954. <https://doi.org/10.1093/nar/gkj485>.
- 17 Rankin S, Reszka AP, Huppert J, et al. Putative DNA quadruplex formation within the human c-kit oncogene. *J Am Chem Soc.* 2005;127:10584–10589. <https://doi.org/10.1021/ja050823u>.
- 18 Fernando H, Reszka AP, Huppert J, et al. A conserved quadruplex motif located in a transcription activation site of the human c-kit oncogene. *Biochemistry-US.* 2006;45:7854–7860. <https://doi.org/10.1021/bi0601510>.
- 19 Guo K, Pourpak A, Beetz-Rogers K, Gokhale V, Sun D, Hurley LH. Formation of pseudosymmetrical G-quadruplex and i-motif structures in the proximal promoter region of the RET oncogene. *J Am Chem Soc.* 2007;129:10220–10228. <https://doi.org/10.1021/ja072185g>.
- 20 Palumbo SL, Ebbinghaus SW, Hurley LH. Formation of a unique end-to-end stacked pair of G-quadruplexes in the hTERT core promoter with implications for inhibition of telomerase by G-quadruplex-interactive ligands. *J Am Chem Soc.* 2009;131:10878–10891. <https://doi.org/10.1021/ja902281d>.
- 21 Brooks TA, Hurley LH. The role of supercoiling in transcriptional control of MYC and its importance in molecular therapeutics. *Nat Rev Cancer.* 2009;9:849–861. <https://doi.org/10.1038/nrc2733>.
- 22 Yang D, Okamoto K. Structural insights into G-quadruplexes: towards new anticancer drugs. *Future Med Chem.* 2010;2:619–646. <https://doi.org/10.4155/fmc.09.172>.
- 23 Qin Y, Hurley LH. Structures, folding patterns, and functions of intramolecular DNA G-quadruplexes found in eukaryotic promoter regions. *Biochimie.* 2008;90:1149–1171. <https://doi.org/10.1016/j.biochi.2008.02.020>.
- 24 Gehring K, Leroy JL, Gueron M. A tetrameric DNA structure with protonated cytosine-cytosine base pairs. *Nature.* 1993;363:561–565. <https://doi.org/10.1038/363561a0>.
- 25 Day HA, Pavlou P, Waller ZA. i-Motif DNA: structure, stability and targeting with ligands. *Bioorg Med Chem.* 2014;22:4407–4418. <https://doi.org/10.1016/j.bmc.2014.05.047>.
- 26 Zeraati M, Langley DB, Schofield P, et al. I-motif DNA structures are formed in the nuclei of human cells. *Nat Chem.* 2018;10:631–637. <https://doi.org/10.1038/s41557-018-0046-3>.
- 27 Choi J, Kim S, Tachikawa T, Fujitsuka M, Majima T. pH-induced intramolecular folding dynamics of i-motif DNA. *J Am Chem Soc.* 2011;133:16146–16153. <https://doi.org/10.1021/ja2061984>.
- 28 Dettler JM, Buscaglia R, Cui J, Cashman D, Blynn M, Lewis EA. Biophysical characterization of an ensemble of intramolecular i-motifs formed by the human c-MYC NHE IIII P1 promoter mutant sequence. *Biophys J.* 2010;99:561–567. <https://doi.org/10.1016/j.bpj.2010.04.042>.
- 29 Lieblein AL, Buck J, Schlepckow K, Furtig B, Schwalbe H. Time-resolved NMR spectroscopic studies of DNA i-motif folding reveal kinetic partitioning. *Angew Chem Int Ed Engl.* 2012;51:250–253. <https://doi.org/10.1002/anie.201104938>.
- 30 Lieblein AL, Kramer M, Dreuw A, Furtig B, Schwalbe H. The nature of hydrogen bonds in cytidine...H+...cytidine DNA base pairs. *Angew Chem Int Ed Engl.* 2012;51:4067–4070. <https://doi.org/10.1002/anie.201200549>.
- 31 Wright EP, Huppert JL, Waller Z. Identification of multiple genomic DNA sequences which form i-motif structures at neutral pH. *Nucleic Acids Res.* 2017;45:2951–2959. <https://doi.org/10.1093/nar/gkx090>.
- 32 Li X, Peng Y, Ren J, Qu X. Carboxyl-modified single-walled carbon nanotubes selectively induce human telomeric i-motif formation. *Proc Natl Acad Sci USA.* 2006;103:19658–19663. <https://doi.org/10.1073/pnas.0607245103>.
- 33 Day HA, Huguin C, Waller ZA. Silver cations fold i-motif at neutral pH. *Chem Commun (Camb).* 2013;49:7696–7698. <https://doi.org/10.1039/c3cc43495h>.
- 34 Kendrick S, Kang HJ, Alam MP, et al. The dynamic character of the BCL2 promoter i-motif provides a mechanism for modulation of gene expression by compounds that bind selectively to the alternative DNA hairpin structure. *J Am Chem Soc.* 2014;136:4161–4171. <https://doi.org/10.1021/ja410934b>.
- 35 Chen Y, Qu K, Zhao C, et al. Insights into the biomedical effects of carboxylated single-wall carbon nanotubes on telomerase and telomeres. *Nat Commun.* 2012;3:1074. <https://doi.org/10.1038/ncomms2091>.
- 36 Gonzalez V, Hurley LH. The c-MYC NHE III(1): function and regulation. *Annu Rev Pharmacol Toxicol.* 2010;50:111–129. <https://doi.org/10.1146/annurev.pharmtox.48.113006.094649>.
- 37 Brown RV, Wang T, Chappeta VR, et al. The Consequences of Overlapping G-Quadruplexes and i-Motifs in the Platelet-Derived Growth Factor Receptor beta Core Promoter Nucleases Hypersensitive Element Can Explain the Unexpected Effects of Mutations and Provide Opportunities for Selective Targeting of Both Structures by Small Molecules To Downregulate Gene Expression. *J Am Chem Soc.* 2017;139:7456–7475. <https://doi.org/10.1021/jacs.6b10028>.
- 38 Guo K, Gokhale V, Hurley LH, Sun D. Intramolecularly folded G-quadruplex and i-motif structures in the proximal promoter of the vascular endothelial growth factor gene. *Nucleic Acids Res.* 2008;36:4598–4608. <https://doi.org/10.1093/nar/gkn380>.
- 39 Benabou S, Ferreira R, Avino A, et al. Solution equilibria of cytosine- and guanine-rich sequences near the promoter region of the n-myc gene that contain stable hairpins within lateral loops. *BBA.* 1840;2014:41–52. <https://doi.org/10.1016/j.bbagen.2013.08.028>.
- 40 Shu B, Cao J, Kuang G, et al. Syntheses and evaluation of new acridone derivatives for selective binding of oncogene c-myc promoter i-motifs in gene transcriptional regulation. *Chem Commun (Camb).* 2018;54:2036–2039. <https://doi.org/10.1039/c8cc00328a>.
- 41 Hu MH, Chen SB, Wang B, et al. Specific targeting of telomeric multimeric G-quadruplexes by a new triaryl-substituted imidazole. *Nucleic Acids Res.* 2017;45:1606–1618. <https://doi.org/10.1093/nar/gkw1195>.
- 42 Elmes RBP, Orange KN, Cloonan SM, Williams DC, Gunnlaugsson T. Luminescent Ruthenium(II) Polypyridyl Functionalized Gold Nanoparticles; Their DNA Binding Abilities and Application As Cellular Imaging Agents. *J Am Chem Soc.* 2011;133:15862–15865. <https://doi.org/10.1021/ja2061159>.
- 43 Van Vliet LD, Ellis T, Foley PJ, et al. Molecular recognition of DNA by rigid [n]-polynorborene-derived bifunctional intercalators: Synthesis and evaluation of their binding properties. *J Med Chem.* 2007;50:2326–2340. <https://doi.org/10.1021/jm0613020>.
- 44 Banerjee S, Kitchen JA, Bright SA, et al. Synthesis, spectroscopic and biological studies of a fluorescent Pt(II) (terpy) based 1,8-naphthalimide conjugate as a DNA targeting agent. *Chem Commun.* 2013;49:8522–8524. <https://doi.org/10.1039/c3cc44962a>.

- 45 Chen XC, Chen SB, Dai J, et al. Tracking the Dynamic Folding and Unfolding of RNA G-Quadruplexes in Live Cells. *Angew Chem Int Ed Engl.* 2018;57:4702–4706. <https://doi.org/10.1002/anie.201801999>.
- 46 Andrae J, Gallini R, Betsholtz C. Role of platelet-derived growth factors in physiology and medicine. *Gene Dev.* 2008;22:1276–1312. <https://doi.org/10.1101/gad.1653708>.
- 47 Ostman A, Heldin C. PDGF receptors as targets in tumor treatment. In: VandeWoude GF, Klein G, eds. *Advances in Cancer Research.* vol. 97. 2007:247–274.
- 48 Govindarajan B, Shah A, Cohen C, et al. Malignant transformation of human cells by constitutive expression of platelet-derived growth factor-BB. *J Biol Chem.* 2005;280:13936–13943. <https://doi.org/10.1074/jbc.M500411200>.
- 49 Heldin CH, Rubin K, Pietras K, Ostman A. High interstitial fluid pressure - An obstacle in cancer therapy. *Nat Rev Cancer.* 2004;4:806–813. <https://doi.org/10.1038/nrc1456>.
- 50 Furuhashi M, Sjöblom T, Abramsson A, et al. Platelet-derived growth factor production by B16 melanoma cells leads to increased pericyte abundance in tumors and an associated increase in tumor growth rate. *Cancer Res.* 2004;64:2725–2733. <https://doi.org/10.1158/0008-5472.CAN-03-1489>.
- 51 Kang H, Kendrick S, Hecht SM, Hurley LH. The Transcriptional Complex Between the BCL2 i-Motif and hnRNP LL Is a Molecular Switch for Control of Gene Expression That Can Be Modulated by Small Molecules. *J Am Chem Soc.* 2014;136:4172–4185. <https://doi.org/10.1021/ja4109352>.
- 52 Zhang Y, Feng S, Wu Q, et al. Microwave-assisted synthesis and evaluation of naphthalimides derivatives as free radical scavengers. *Med Chem Res.* 2011;20:752–759. <https://doi.org/10.1007/s00044-010-9384-4>.
- 53 Sawa M, Hsu TL, Itoh T, et al. Glycoproteomic probes for fluorescent imaging of fucosylated glycans in vivo. *Proc Natl Acad Sci USA.* 2006;103:12371–12376. <https://doi.org/10.1073/pnas.0605418103>.
- 54 Rogers JE, Kelly LA. Nucleic acid oxidation mediated by naphthalene and benzophenone imide and diimide derivatives: Consequences for DNA redox chemistry. *J Am Chem Soc.* 1999;121:3854–3861. <https://doi.org/10.1021/ja9841299>.
- 55 Alcalá MA, Kwan SY, Shade CM, et al. Luminescence targeting and imaging using a nanoscale generation 3 dendrimer in an in vivo colorectal metastatic rat model. *Nanomed-Nanotechnol.* 2011;7:249–258. <https://doi.org/10.1016/j.nano.2010.09.002>.
- 56 Parkesh R, Lee TC, Gunnlaugsson T. Fluorescence imaging of bone cracks (microdamage) using visibly emitting 1,8-naphthalimide-based PET sensors. *Tetrahedron Lett.* 2009;50:4114–4116. <https://doi.org/10.1016/j.tetlet.2009.04.115>.
- 57 Xiao H, Chen M, Shi G, Wang L, Yin H, Mei C. A novel fluorescent molecule based on 1,8-naphthalimide: synthesis, spectral properties, and application in cell imaging. *Res Chem Intermediat.* 2010;36:1021–1026. <https://doi.org/10.1007/s11164-010-0214-6>.
- 58 Jindal DP, Bedi V, Jit B, et al. Synthesis and study of some new N-substituted imide derivatives as potential anticancer agents. *Farmaco (Lausanne).* 2005;60:283–290. <https://doi.org/10.1016/j.farmac.2005.01.011>.
- 59 Galunov NZ, Krasovitskii BM, Lyubenko ON, Yermolenko IG, Patsenker LD, Doroshenko AO. Spectral properties and applications of the new 7H-benzo[de]pyrazolo[5,1-a]isoquinolin-7-ones. *J Lumin.* 2003;102:119–124. [https://doi.org/10.1016/S0022-2313\(02\)00477-5](https://doi.org/10.1016/S0022-2313(02)00477-5).
- 60 Stolarski R. Fluorescent Naphthalimide Dyes for Polyester Fibres. *Fibres Text East Eur.* 2009;17:91–95.
- 61 Goswami S, Sen D, Das NK, Hazra G. Highly selective colorimetric fluorescence sensor for Cu²⁺: cation-induced 'switching on' of fluorescence due to excited state internal charge transfer in the red/near-infrared region of emission spectra. *Tetrahedron Lett.* 2010;51:5563–5566. <https://doi.org/10.1016/j.tetlet.2010.08.048>.
- 62 Lv Y, Cao M, Li J, Wang J. A Sensitive Ratiometric Fluorescent Sensor for Zinc(II) with High Selectivity. *Sensors-Basel.* 2013;13:3131–3141. <https://doi.org/10.3390/s130303131>.
- 63 Georgiev NI, Bojinov VB, Nikolov PS. The design, synthesis and photophysical properties of two novel 1,8-naphthalimide fluorescent pH sensors based on PET and ICT. *Dyes Pigments.* 2011;88:350–357. <https://doi.org/10.1016/j.dyepig.2010.08.004>.
- 64 Ferreira R, Remon P, Pischel U. Multivalued Logic with a Tristable Fluorescent Switch. *J Phys Chem C.* 2009;113:5805–5811. <https://doi.org/10.1021/jp809527d>.
- 65 Gan JA, Song QL, Hou XY, Chen KC, Tian H. 1,8-Naphthalimides for non-doping OLEDs: the tunable emission color from blue, green to red. *J Photoch Photobio A.* 2004;162:399–406. [https://doi.org/10.1016/s1010-6030\(03\)00381-2](https://doi.org/10.1016/s1010-6030(03)00381-2).
- 66 Kolosov D, Adamovich V, Djurovich P, Thompson ME, Adachi C. 1,8-naphthalimides in phosphorescent organic LEDs: The interplay between dopant, exciplex, and host emission. *J Am Chem Soc.* 2002;124:9945–9954. <https://doi.org/10.1021/ja0263588>.
- 67 Jung SO, Yuan W, Ju JU, et al. A New Orange-Light-Emitting Materials Based on (N-naphthyl)-1,8-naphthalimide for OLED Applications. *Mol Cryst Liq Cryst.* 2009;514:375–384. <https://doi.org/10.1080/15421400903217751>.